[redacted]

DESIGN, CONSTRUCTION AND EVALUATION OF A SUBSONIC WIND TUNNEL

by

MILAN VLAJINAC

S.B., Massachusetts Institute of Technology

(1966)

SUBMITTED IN PARTIAL FULFILLMENT

OF THE REQUIREMENTS FOR THE

DEGREE OF MASTER OF SCIENCE

at the

MASSACHUSETTS INSTITUTE OF TECHNOLOGY

June, 1970

Signature of Author Milan Vlajinac

Department of Aeronautics
and Astronautics, June 1970

Certified by _____

Thesis Supervisor

Accepted by _____

Chairman, Departmental
Graduate Committee

DESIGN, CONSTRUCTION AND EVALUATION OF A SUBSONIC WIND TUNNEL

by

Milan Vlajinac

Submitted to the Department of Aeronautics and Astronautics on June 4, 1970 in partial fulfillment of the requirements for the degree of Master of Science.

ABSTRACT

The design, construction and calibration of a subsonic wind tunnel is summarized. The design philosophy is discussed and methods for wind tunnel calculations are outlined. Comparison of measured wind tunnel parameters are shown to be in excellent agreement with design calculations.

Thesis Supervisor: Eugene E. Covert

Title: Professor of Aeronautics and Astronautics

ACKNOWLEDGEMENTS

The author wishes to thank Professor Morton Finston for making this thesis possible through the use of the facilities of the Aerophysics Laboratory.

Special thanks are due to Professor Eugene E. Covert for the hours of patient discussion, his excellent suggestions, and encouragement offered during the course of this thesis.

The author is grateful to Timothy Stephens, Jim Coffin and many other members of the laboratory personnel for the many hours of technical assistance.

For the final preparation of this thesis, the author wishes to thank Helen Putnam, Cathy Callahan and Linda Wainionpaa.

This work was carried out under the sponsorship of the Full-Scale Research Division, NASA-Langley Research Center, Hampton, Virginia, under Contract NAS1-4421. This contract was monitored by Mr. Harleth Wiley of the NASA-Langley Vehicle-Dynamics Section.

TABLE OF CONTENTS

TABLE OF CONTENTS (continued)

TABLE OF CONTENTS (continued)

TABLE OF CONTENTS (continued)

TABLE OF CONTENTS (continued)

SYMBOLS

A	area
A,B	constants
a	speed of sound
C	perimeter
C_D	Drag coefficient $\frac{\text{DRAG FORCE}}{q}$
D	diameter
D_h	hydraulic diameter $(\frac{4A}{C})$
E	flow kinetic energy
E.R.	energy ratio
e	hot wire voltage
i	hot wire current
K	screen pressure loss coefficient
k	pressure loss coefficient $\frac{\Delta P}{q}$
L	length
M	Mach number
P	power
q	dynamic pressure 1/2 ρV^2
R	hot wire resistance
Re	Reynolds number $\frac{\rho V}{\mu}$
R_g	hot wire cold resistance
r	resistance fluctuation

SYMBOLS (continued)

T	turbulence level
T.F.	turbulence factor
V	velocity
$\overline{V}$	mean velocity
$\overline{V^2}$	mean square velocity
V_x, V_y, V_z	fluctuation velocity components
α	diffuser divergence angle
E	energy loss
P	pressure loss
P_{set}	speed setting pressure
λ	friction factor
ε	power loss factor
η	fan efficiency
ρ	density
γ	specific heat ratio

Subscripts

o	test section conditions
i	integers

CHAPTER 1

INTRODUCTION

1.1 General Considerations and Requirements

The evolution of the second generation magnetic balance[1] at the M.I.T. Aerophysics Laboratory indicated the need for a small subsonic wind tunnel which would be simple to operate and could simulate the aerodynamic loads (similar dynamic pressure) on models tested in the supersonic (M = 4.25) facility. The immediate advantage of such a wind tunnel would be to provide the initial operational experience and evaluation of the magnetic balance at a considerably reduced operating cost. The goal in the construction of this wind tunnel was to incorporate into its design as many desirable features as possible in order to make it a high efficiency, low turbulence wind tunnel for general laboratory use.

The principal geometric requirement for the tunnel was that the test section be compatible with the magnetic balance "test" region. This limited the maximum test section size to 7 1/2 inches in diameter. In addition, the area in which the wind tunnel would be located restricted the overall tunnel length to less than 35 feet. An open circuit tunnel configuration was chosen both for simplicity in construction as well as the reduction in overall size by omission of the flow return duct. A practical consideration in a closed circuit wind tunnel design is the addition of a method for cooling the air in the tunnel circuit[2]. Since this tunnel was to be installed in a reasonably large test room, this aspect of the design was unnecessary.

The dynamic pressure in the test section was originally chosen to be 1.5 p.s.i. as a basis for power requirement and performance calculations. This value corresponded to the maximum dynamic pressure of the Hypersonic Flow Apparatus at NASA Langley at which a magnetic balance installation was proposed. From these calculations and cost considerations the maximum tunnel dynamic pressure was extended above this value for the particular fan and power plant selection that matched the calculated wind tunnel requirements.

1.2 Components of an Open Circuit Wind Tunnel

The principal parts of an open circuit wind tunnel are shown in figure 1. A functional description of the various components follows.

i., Effuser. The effuser is located ahead of the test section and should consist in part of a large constant area region known as the stilling section. This is followed by a contraction section, where the flow is accelerated to its maximum value at the test section. The stilling section, because of the low flow velocity in it, is a practical location for placing screens and honeycomb to reduce the flow irregularities which eventually go through the test section. The contraction section should create a continuously increasing flow velocity along its length.

ii.) Test Section. The test section should be the region of maximum tunnel velocity and is where models are normally tested. It should be easily accessible as well as provide viewing access to the model being tested. It is desirable to obtain uniform steady flow velocity along the test section length and a minimum variation of the axial velocity across the test section.

iii.) Diffuser. Downstream of the test section the flow should be decelerated as efficiently as possible in order to minimize the loss of flow kinetic energy. Particular effort should be made to avoid flow separation in the diffuser, which

can markedly decrease its efficiency and affect the overall tunnel performance.

iv.) Power Plant. For subsonic tunnels the power plant usually consists of a fan driven by an electric motor. It provides the necessary pressure rise to overcome the loss in pressure in the tunnel circuit. The proper choice of fan and motor is required in order to obtain efficient tunnel operation.

CHAPTER 2

WIND TUNNEL DESIGN CONSIDERATIONS

2.1 Power Requirements

The power required to maintain steady flow through the wind tunnel is equal to the total losses occurring in the flow through the tunnel. These losses are due to kinetic energy being dissipated by vorticity and turbulence. The loss in kinetic energy, which appears as a decrease in total pressure, must be compensated by a pressure rise, usually provided by a fan. Thus, if the power input to the fan is P (i.e. motor shaft output) and the fan has an efficiency η, the equation balancing the energy input to the stream to the energy losses in the tunnel is

$$\eta P = \sum \text{circuit losses} \tag{2.1}$$

As has been pointed out in reference 2, the tunnel can be divided into sections with the energy loss of each section written as a drop in pressure Δp or a pressure drop coefficient $k_i = \Delta P_i / q_o$ where q_o is test section dynamic pressure ($1/2\ \rho_o V_o^2$). The flow energy through the test section is

$$E_o = \tfrac{1}{2} \rho_o A_o V_o^3 \tag{2.2}$$

The energy loss in each tunnel section is

$$\Delta E_i = \frac{\Delta P}{g} \left(\tfrac{1}{2} \rho_i A_i V_i \right) \tag{2.3}$$

Substituting equation (2.1)

$$\Delta E_i = \frac{K_i \left(\frac{1}{2}\rho_o V_o^2\right)}{\frac{1}{2}\rho_i V_i^2} \left(\frac{1}{2}\rho_i A_i V_i^3\right) \tag{2.4}$$

$$\Delta E_i = K_i \left(\frac{1}{2}\rho_o V_o^2\right) A_i V_i \tag{2.5}$$

The continuity equation is

$$\rho_i V_i A_i = \rho_o V_o A_o \tag{2.6}$$

which gives

$$\Delta E_i = K_i \left(\frac{\rho_o}{\rho_i}\right)\left(\frac{1}{2}\rho_o V_o^3 A_o\right) \tag{2.7}$$

For subsonic flow with $M < .4$, $\frac{\rho_o}{\rho_i} \approx 1$ (within 1%) and equation 2.1 becomes

$$\eta P = \frac{1}{2}\rho_o V_o^3 A_o \sum_i K_i \tag{2.8}$$

The required power for a given test section size and flow conditions depends on the sum of the pressure drop coefficients (K_i) in the various tunnel sections. A reduction in these coefficients improves the tunnel efficiency. A quantity relating to the tunnel performance is the energy ratio defined in reference 3 as

$$E.R. = \frac{\frac{1}{2}\rho_o V_o^3 A_o}{\eta P} = \frac{1}{\sum_i K_i} \tag{2.9}$$

and is a measure of the tunnel efficiency.

2.2 Calculation of Pressure Losses Due to Skin Friction

The methods for predicting pressure losses in ducts due to skin friction have been well documented in the literature[4]. Experimental values of skin friction coefficients are available for various wall roughnesses and thereby enable accurate estimates of pressure losses to be made. The pressure loss for a circular cylinder can be determined by the following formula:

$$\Delta P = \int_0^L \lambda \left(\tfrac{1}{2}\rho V^2\right) \frac{dL}{D} \qquad (2.10)$$

The friction coefficient λ is generally tabulated as a function of the Reynolds number. This is shown in figure 2. In the case of a non-circular cross section one can define a hydraulic diameter $D_h = \frac{4A}{C}$ where A is the cross sectional area and C is the wetted perimeter. It has been shown experimentally[4] that using the hydraulic diameter for non-circular cross sections gives good results with laws for circular pipes in the turbulent regime ($Re_{D_h} > 2000$).

Pope[2] has shown that both wall friction and expansion losses occur in divergent sections. The combined losses for a constant divergence angle α are

$$\Delta P = \tfrac{1}{2}\rho_o V_o^2 \left(\frac{\lambda}{8 \operatorname{TAN} \alpha/2} + 0.6 \operatorname{TAN} \frac{\alpha}{2} \right) \left(1 - \frac{D_1^4}{D_2^4}\right) \frac{D_o^4}{D_2^4} \qquad (2.11)$$

where D_1 = small diameter, D_2 = large diameter, D_o = test section diameter. Differentiation of equation (2.11) leads to an optimum expansion when

$$\operatorname{TAN} \frac{\alpha}{2} = \sqrt{\frac{\lambda}{4.8}} \qquad (2.12)$$

2.3 Additional Pressure Losses

Aside from skin friction losses in the tunnel circuit, the following losses occur.

Damping Screens. Wire screens, which are used for the reduction of turbulence, produce losses in pressure which are dependent on the screen mesh size and diameter of wire used. Pressure drop coefficients for commercially available wire screens are measured as the ratio of the pressure loss through the screen to the local dynamic pressure. Pressure loss coefficient data for various screens is shown in figure 3.

Honeycomb. In addition to screens, honeycomb is sometimes used for reduction of turbulence, particularly transverse velocity fluctuations. Roberts[5] has measured honeycomb losses to be approximately 0.20 times the local dynamic pressure. This value is considerably lower than the recommended pressure loss coefficients for screens.

Diffuser Exit. For an open circuit tunnel an additional pressure loss results from the discharge of the flow kinetic energy at the tunnel exit. The loss is just equal to the dynamic pressure at the diffuser exit.

Corners. Losses that occur at corners or where the flow turns can be computed by methods described in references 2 and 3 which give values of pressure drop coefficients for various types of turning vanes. In open circuit tunnels, corners are not advisable unless the available space is limited.

Model Drag. The effect of a model placed in the test section is usually considered as an additional power requirement rather than a pressure loss. The power required to overcome the drag of a model in the tunnel is[3]

$$\frac{1}{2}\rho V^3 S C_D \varepsilon \qquad (2.13)$$

where S is the model area on which the drag coefficient, C_D, is based. The factor ε allows for the additional power requirements due to the interference of the model on the flow in and downstream of the working section. This factor is normally on the order of 1 but can be as high as 10 in some cases.

2.4 Effects of Wind Tunnel Component Geometry on the Power Required

The required power for a specified test section size and dynamic pressure can be varied by altering the geometry of the remaining wind tunnel components. Since the test section area and length for the proposed tunnel were fixed by geometrical constraints, the effect of various effuser and diffuser geometries on the power required were analyzed. The test section conditions were the following:

Area = 32.6 sq. in.

Length = 36 in.

Dynamic Pressure = 1.5 pounds per square inch

a.) Contraction Section Losses

The losses in the contraction section are due to skin friction and can be computed from formula (2.10). Assuming a constant taper for the contraction and integrating gives

$$\frac{\Delta P}{\frac{1}{2}\rho_o V_o^2} = \frac{\lambda}{4} \frac{L_o}{D_i - D_o} \left(1 - \frac{D_o^4}{D_i^4}\right) \qquad (2.14)$$

where L_o is the length, D_o the test section diameter and D_i the inlet cone diameter. Note that for non-circular sections one can replace the diameters with the hydraulic diameter defined in section 2.2. The results obtained for various contraction ratios $\frac{D_i^2}{D_o^2}$ are shown in figure 4 for both constant length and $L_o = 2D_i$. The contraction cone

length is normally chosen to be twice the inlet diameter. This choice gives a minimum value of loss coefficient for a 30:1 contraction ratio.

b.) Diffuser Losses

The diffuser losses are due to both skin friction and expansion. In order to avoid separation in the diffuser, the maximum divergence angle should be approximately 5° total angle[2]. This value agrees with the optimum expansion angle (equation (2.12)) for a friction factor $\lambda = 0.011$. Calculations of pressure loss coefficients were made for a 5° divergence angle diffuser using equation (2.11). The addition of exit losses results in a total diffuser loss coefficient equal to

$$\frac{\Delta P}{\frac{1}{2}\rho_o V_o^2} = \left(3.14\,\lambda + 0.0262\right)\left(1 - \frac{D_o^4}{D_e^4}\right) + \left(\frac{D_o}{D_e}\right)^2 \qquad (2.15)$$

where D_e is the diffuser exit diameter. Pressure loss coefficients for various exit diameters are shown in figure 5. It can be seen that the pressure loss coefficient decreases at a reduced rate with increasing exit diameter above an exit diameter of approximately 20 inches.

c.) Test Section Losses

The test section loss coefficient for a constant area section using equation (2.10) and a mean value of the friction factor reduces to

$$\frac{\Delta P}{\frac{1}{2}\rho_o V_o^2} = \lambda \frac{L}{D_o} \qquad (2.16)$$

For the test section design chosen at a dynamic pressure of 1.5 lb/sq in, the pressure loss coefficient is

$$\frac{\Delta P}{\frac{1}{2}\rho_o V_o^2} = 0.0584 \qquad (2.17)$$

d.) Stilling Section Losses

The losses in the stilling are primarily due to screens used for turbulence reduction. The recommended screen mesh should give a pressure loss equal to twice the local dynamic pressure (see section 2.5). Here, again, the contraction ratio affects the total wind tunnel pressure loss due to the screens. For a given choice of screen pressure loss coefficient k, the tunnel pressure loss coefficient is

$$\frac{\Delta P}{\frac{1}{2}\rho_o V_o^2} = K\left(\frac{D_o}{D_i}\right)^4 \qquad (2.18)$$

Since the losses are inversely proportional to the square of the contraction ratio, $(\frac{D_i}{D_o})^2$, it is desirable to have a large contraction ratio for power economy.

2.5 Turbulence

One of the most important quantities which affects measurements in a wind tunnel is the turbulence or unsteady motion superimposed on the mean flow. In order that simulation of free flight might be properly made, it is desirable to reduce the turbulence in the test section to a minimum. The effect of increasing the turbulence in the test section is to increase the effective Reynolds number. A higher Reynolds number tends to produce natural turbulence. The boundary layer transition point on a model will move forward with increasing tunnel turbulence and produce a turbulent boundary layer over a larger portion of the model with pronounced changes in the force and moment coefficients. The separation characteristics of some models will be markedly changed with increased tunnel turbulence, particularly at low Reynolds numbers where laminar separation is expected.

The level of turbulence in a wind tunnel can be expressed as the ratio of the mean velocity fluctuations to freestream velocity. For isotropic turbulence the mean velocity fluctuations in the three coordinate directions are equal:

$$\overline{V_x^2} = \overline{V_y^2} = \overline{V_z^2} \tag{2.19}$$

The turbulence level can then be defined as

$$T = \frac{\sqrt{\frac{1}{3}\left(\overline{V_x^2} + \overline{V_y^2} + \overline{V_z^2}\right)}}{V_o} = \frac{\sqrt{\overline{V_x^2}}}{V_o} \tag{2.20}$$

where V_o is the mean tunnel velocity.

The turbulence may be found by measuring the critical Reynolds number of a sphere at which the dra coefficient decreases sharply. This critical Reynolds number of a sphere at which the drag coefficient decreases sharply. This critical Reynolds number depends strongly on the turbulence level in the tunnel. A high intensity of turbulence leads to boundary layer transition at low Reynolds numbers, causing the separation point to move downstream and thus decreasing the wake, which in turn reduces the drag. The critical Reynolds number for a sphere in free flight has been measured to be 385,000. The turbulence factor is defined[2] as

$$T.F. = \frac{385{,}000}{Re_c} \tag{2.21}$$

where Re_c is the critical Reynolds number at which the sphere drag coefficient equals 0.30. The effective Reynolds number, Re_e, in the test section is defined as

$$Re_e = (T.F.)\,Re \tag{2.22}$$

The effective Reynolds number thus increases with increasing turbulence level. The relation between the turbulence factor and turbulence level is shown in figure 6. The turbulence level can be measured using hot wire techniques. These are described in a later section.

2.6 Turbulence Reduction

The conventional methods for reducing the turbulence level in the test section involve the use of screens and honeycomb. The effect of a screen on the turbulence is dependent on the screen pressure loss coefficient K defined as

$$K = \frac{\Delta P}{\frac{1}{2}\rho V^2} \tag{2.23}$$

where ΔP is the pressure drop across the screen and $1/2\ \rho V^2$ is the dynamic pressure of the flow through the screen. Collar[6] has shown that the fluctuating axial component of velocity, V_x, is reduced as

$$\frac{V_x'}{V_x} = \frac{2-K}{2+K} \tag{2.24}$$

where V'_x is the fluctuating velocity downstream of the screen and V_x the fluctuating velocity ahead of the screen. The fluctuating component disappears downstream of the screen for K = 2.0. Batchelor[7] has shown that the mean square velocity fluctuations, whose mean is zero, decrease as

$$\frac{\overline{V_x'^2}}{\overline{V_x^2}} = \left(\frac{1-2/5\,K}{1+2/5\,K}\right)^2 \tag{2.25}$$

where $\overline{V_x^2}$ and $\overline{V_x'^2}$ are the mean square axial turbulent fluctuations upstream and downstream of the screens, respectively. From this $\overline{V_z^2}$ vanishes for K = 2.5 which is comparable to that required for steady flow. A similar expression for the transverse components is

$$\frac{\overline{V_y'^2}}{\overline{V_y^2}} = \frac{\overline{V_z'^2}}{\overline{V_z^2}} = \left(1 - \frac{K}{10(1+2/5\,K)}\right)^2 \tag{2.26}$$

which indicates that the transverse components are less reduced than the axial component. Dryden and Shubauer[8] have shown experimentally that the intensity of turbulence is reduced by

$$\frac{T'}{T} = \frac{1}{\sqrt{1+K}} \tag{2.27}$$

They have also shown that the turbulence is further reduced if several screens are used with the same total pressure drop as for one screen. If n is the number of screens, each with a pressure drop K, the turbulence is reduced by

$$\frac{T'}{T} = \frac{1}{(1+K)^{n/2}} \tag{2.28}$$

as compared to

$$\frac{T'}{T} = \frac{1}{(1+nK)^{1/2}} \tag{2.29}$$

for a single screen with the same total loss coefficient. It is therefore advisable to use several screens for a given total pressure drop coefficient.

The use of honeycomb in reducing the wind tunnel turbulence appears to be primarily effective in reducing the transverse components of velocity fluctuation, more so than the axial components. This tends to complement the lesser effectiveness of the screens to reduce the transverse components of velocity fluctuations (equation (2.26)).

The combined use of screens and honeycomb will provide a reduction of turbulence in the tunnel. Their location should be in the region of least velocity, ahead of the test section both to reduce the tunnel pressure losses and the unit Reynolds number in that region.

2.7 Test Section Boundary Layer Growth

Due to the growth of the boundary layer on the test section walls, the flow velocity will increase along the length of the test section for a constant area test section. If

uniform velocity distribution is desirable along the test section length, the cross-section area must be gradually increased along its length to allow for the boundary growth on the walls. The divergence of the walls should be equal to the boundary layer displacement thickness (δ^*).

Experimental data for obtaining values of boundary layer displacement thickness versus length for various Reynolds numbers are tabulated in reference 3. It should be noted that a choice of wall divergence will be proper for only one test Reynolds number. A constant taper is usually used for the entire test section based on a mean value of Reynolds number.

CHAPTER 3

WIND TUNNEL CONSTRUCTION

3.1 Construction of Wind Tunnel Components

An open circuit wind tunnel was designed and constructed incorporating features discussed in Chapter 2. The assembled wind tunnel attached to the magnetic balance is shown in figure 7. A sketch of the assembled tunnel in figure 8 shows the overall dimensions and components. A brief description of the tunnel components, as well as the Aerophysics Laboratory drawing numbers, is given below.

a.) Test Section (D-8-868, D-8-871, D-8,873, D-8-883)

The test section was designed to be compatible with the magnetic balance. Transparent plexiglass was used in its construction to provide viewing of the model. An octagonal cross section was chosen to optimize the available space inside the balance while at the same time providing plane surfaces on the walls to eliminate optical distortion of the model. The test section has a constant taper on its walls to allow for boundary layer growth. The test section is supported inside the magnetic balance with flanges attached at either end of the balance. A frame was constructed to hold these flanges when the tunnel is operated without the magnetic balance.

b.) Contraction Section and Stilling Section (Dwgs E-8-872, D-8-869, D-8-880)

The contraction section and stilling section were made of wood (pine), and both have octagonal cross sections. A 20:1 contraction ratio section was designed using contours

similar to those recommended by Tsien[9] at the small end of the contraction section. The stilling section contains three screens (20-mesh, 0.016 in. wire) and a 2-inch long honeycomb section with 1/4-inch cells. The stilling section has a faired inlet to avoid an abrupt boundary to the incoming flow. Both sections are mounted on a stand with roller tracks to permit fore and aft movement with respect to the test section. The contraction section is joined to the test section by a mating flange and three snap-clamps which compress an O-ring, thereby sealing the joint. Forward movement of the inlet section provides access to the test section.

c.) Diffuser (Dwg E-8-881)

The diffuser was made of wood (mahogany) and is octagonal in cross section. A constant divergence angle of 5° between opposing walls was used. The diffuser attaches to the downstream test section flange. The diffuser exit matches the fan inlet with a 9.5 in. inscribed radius. Coupling between the diffuser exit and fan inlet is accomplished by the use of two inflated rubber tubes which are compressed between flanges on the fan and diffuser. This provides an air-tight seal between the two as well as vibration isolation. Three access hatches are located along the diffuser, and a coarse screen (2-mesh) is located at the diffuser end to protect the fan.

d.) Power Plant (Dwg D-8-885)

A centrifugal blower driven by a 20 h.p. direct-current motor provides the power to the tunnel. The blower is mounted on an elevated platform with the fan discharging through the platform and into a baffle.

3.2 Power Requirement Estimate

The power requirements for the tunnel were calculated using the methods described in Chapter 2. The required power for various mass flow rates through the test section is shown in figure 9. The tunnel maximum dynamic pressure

could be increased from 1.5 lb/sq. in. to 2.5 lb/sq. in. with a 10% cost increase for the driving unit. The additional power versus mass flow rates for the extended tunnel operation is also shown in figure 9. The required fan pressure rise versus mass flow is shown in figure 10.

3.3 Wind Tunnel Energy Ratio Estimate

The tunnel energy ratio defined in equation (2.9) is shown in figure 11 for various mass flow rates.

3.4 Fan Selection

The fan chosen for this tunnel is a centrifugal fan, type No. 20 SISW, made by the Chicago Blower Corporation. The operating characteristics of the fan are shown in figure 12, as well as the estimated tunnel operating requirements.

3.5 Motor Selection

A 20 h.p. direct-current motor was selected to drive the centrifugal blower. The motor is a type CD-85 made by the General Electric Company. The maximum speed for this motor is 3600 r.p.m.

3.6 Construction of Power Supply and Motor Speed Control

In order to have motor speed control from zero to 3600 revolutions per minute, two separate power supplies were designed. The supplies provide a variable voltage to the motor armature and field windings, respectively. The motor windings for the type used in this wind tunnel have a "stabilized shunt" arrangement shown in figure 13. The motor speed can be increased by increasing the armature current or decreasing the field current. The power supply block diagram is shown in figure 14 and was designed to convert the available 3-phase 440 volt power line into two variable voltage direct-current power supplies for the motor. The power supplies are described below.

a.) Motor Armature Power Supply

The power supply for the armature windings can provide a maximum of 230 volts at 115 amperes direct current to the windings. The output voltage can be varied from 0 - 230 volts by manually rotating a wheel attached to a 3-phase variable transformer.

b.) Motor Field Power Supply

The power supply for the motor field windings can provide a maximum of 230 volts at 0.835 amperes direct current to the windings. In order to increase the motor speed beyond the base speed of 1750 r.p.m., a series variable rheostat is used to decrease the field current, thereby increasing the motor speed to 3600 r.p.m.

c.) Control Circuit For Power Supply

A control network was designed for the motor power supply to provide the safety features needed to prevent overloading of any part of the circuit. The control network circuit diagram is shown in figure 15.

d.) Motor Tachometer

A tachometer is coupled to the motor shaft to provide the motor (and fan) speed. The motor speed can be read on the power supply console by means of a voltmeter. A calibration of motor speed versus tachometer voltage is shown in figure 16.

CHAPTER 4

WIND TUNNEL MEASUREMENTS AND CALIBRATION

4.1 Initial Operation

Following the assembly of the various tunnel components, a series of tests were performed to obtain a tunnel calibration and evaluation of its performance. Preliminary measurements indicated that a static pressure of approximately 2.5 $lb/in.^2$ below ambient pressure could be obtained at maximum fan speed. This value was useful in determining the necessary range of pressure-measuring equipment needed for the tunnel calibration.

4.2 Static Pressure Measurements

The test section static pressure was measured along its length by means of nine static pressure orifices in the test section wall. The static pressure orifices were .020 in. diameter holes drilled through the test section walls and equispaced 4 in. apart along the test section length. A 0.125 in. diameter spotface 0.188 in. deep on the test section outside surface was made with copper tubing (0.50 in. long) epoxied into each spotface. The static pressure at each station was read on a 50-inch manometer rack.

4.3 Total Pressure Measurements

The total, or stagnation, pressure in the test section was measured with a pitot tube rake which spanned the test section. The rake consisted of seven pitot tubes spaced 1 in. apart and made from 0.35 diameter hypodermic tubing. The rake could be attached at various locations along the test section wall. The pitot rake was attached to a manometer

bank with which the variation of total pressure across the test section could be measured.

4.4 Dynamic Pressure Measurement

The test section dynamic pressure can be obtained from knowledge of the total and static pressure in the test section. Using the isentropic relations for steady flow, one obtains the following equation[10] for the flow Mach number

$$M^2 = \frac{2}{\gamma-1}\left\{\left(\frac{P_o}{P_s}\right)^{\frac{\gamma-1}{\gamma}} - 1\right\} \qquad (4.1)$$

where P_o is the total pressure, P_s the static pressure and α the specific heat ratio (for air $\gamma = 1.4$). Substituting the following relations

$$\frac{\gamma P}{\rho} = a^2 = \frac{V^2}{M^2} \qquad (4.2)$$

one obtains

$$\frac{P_o - P_s}{\frac{1}{2}\rho V^2} = \frac{2}{\gamma M^2}\left\{\left(\frac{\gamma-1}{2}M^2+1\right)^{\frac{\gamma}{\gamma-1}} - 1\right\} \qquad (4.3)$$

where $1/2\ \rho v^2$ is the dynamic pressure. For values of M less than $\sqrt{2/(\gamma-1)}$ equation (4.3) can be expanded to give

$$\frac{P_o - P_s}{\frac{1}{2}\rho V^2} = \left(1 + \frac{M^2}{4} + \frac{(2-\gamma)M^4}{24} + \frac{(2-\gamma)(3-2\gamma)M^6}{192} + \ldots\right) \qquad (4.4)$$

Using $\gamma = 1.4$ for air one obtains

$$\frac{P_o - P_s}{\frac{1}{2}\rho V^2} = \left(1 + \frac{M^2}{4} + \frac{M^4}{40} + \frac{M^6}{1600} + \ldots\right) \qquad (4.5)$$

As the Mach number approaches zero, the above equation reduces to the incompressible Bernoulli equation

$$P_o - P_s = \frac{1}{2}\rho V^2 \qquad (4.6)$$

An interesting result from equation (4.4) is that, for Mach numbers up to 0.6, the right hand side of the equation varies linearly with the ratio P_o/P_s to within 0.5%. The equation for the dynamic pressure reduces to

$$\frac{1}{2}\rho V^2 = \frac{P_o - P_s}{0.347\, P_o/P_s + 0.653} \quad ; M \leq 0.6 \qquad (4.7)$$

which is expressed as a function of only the total and static pressures.

4.5 Dynamic Pressure Variation Across Test Section

Using the pitot tube rake, the dynamic pressure variation across the test section was measured at the test section inlet and exit. The variation of dynamic pressure at the two stations is shown in figure 17. The maximum variation at both stations is within 0.2% of the mean dynamic pressure.

4.6 Axial Dynamic Pressure Variation

The dynamic pressure was measured at the test section axial position corresponding to the location inlet static pressure tap (X = -16 in.) and exit static pressure tap (X = +16 in.). The difference between the inlet and exit dynamic pressure is shown in figure 18 as a percent of the dynamic pressure at the center (X = 0). The dynamic pressure along the test section decreases in the downstream direction, indicating a slight overexpansion of the test section walls. The variation of dynamic pressure from inlet to exit is approximately 2% at the maximum tunnel dynamic pressure. This corresponds to a variation of 0.063% per inch in dynamic pressure. The overexpansion of the test section walls can be remedied, if necessary, by the addition of taper strips along the test section corners.

4.7 Test Section Speed Setting

In order to determine the dynamic pressure through the test section while a model is being tested, it is impractical

to insert a pitot-static tube into the tunnel, since it would both interfere with the flow over the model and its reading would be affected by the presence of the model. A standard method to determine the test section dynamic pressure is by measuring the difference in static pressure between two locations on the contraction section. Once the relation between the taps on the contraction section and the test section dynamic pressure is obtained, the tunnel speed can be determined in subsequent tests by measurement of the static pressure difference.

Two pressure taps were installed in the contraction section, and a micromanometer was used to measure the pressure difference. The micromanometer fluid used was "Meriam Red." A calibration of this fluid is shown in figure 19. The resolution of the micromanometer is 0.001 in. The test section dynamic pressure was measured at its centerline (X = 0) using the methods described in sections 4.2, 4.3 and 4.4. The test section dynamic pressure versus static pressure difference (ΔP_{set}) is shown in figure 20. A second order equation was fitted to the calibration to give the following relation for test section dynamic pressure in lb/sq. in.

$$\frac{1}{2}\rho_o V_o^2 = 7.232(\Delta P_{set.}) + 4.326(\Delta P_{set.})^2 \qquad (4.8)$$

where ΔP_{set} is in lb/sq. in. The pressure difference in lb/sq. in. is obtained by multiplying the appropriate fluid density (from figure 19) by the measured height of manometer fluid.

The maximum test section dynamic pressure is approximately 2.6 lb/sq. in. for zero blockage.

4.8 Wind Tunnel Speed Resolution

The power supply for motor speed control can provide con-

tinuous variation of fan speed from less than 2 r.p.m. to 3000 r.p.m. Adequate control of motor speed changes can be obtained using the 20-inch wheel on the motor speed control

with approximately 180° rotation for maximum tunnel speed. This corresponds to approximately 3 ft/sec/degree.

The micromanometer used for speed setting provides a measurement of test section dynamic pressure with a resolution of ±0.0005 $lb/in.^2$. This corresponds to an error in velocity of ±7.8 ft/sec.

4.9 Turbulence Measurements

The turbulence level in the test section was measured using a hot wire method. A detailed description of the equipment used and data reduction is presented in Apperdix A. The measured turbulence is shown in figure 21 for several tunnel speeds. It should be noted that the measurements were made with a single wire, so that the measured turbulence represents only the longitudinal and vertical velocity fluctuations due to the orientation of the wire. Denoting the axial and vertical velocity fluctuation by $\overline{v_x^2}$ and $\overline{v_z^2}$, the measured fluctuation is

$$\frac{\sqrt{\overline{v^2}}}{V_o} = \frac{\sqrt{v_x^2 + v_z^2}}{V_o} \qquad (4.9)$$

For isotropic turbulence in the test section, as defined in section 2.5, the turbulence level would be

$$T_{ISOTROPIC} = 0.707 \frac{\sqrt{\overline{v^2}}}{V_o} \qquad (4.10)$$

The measurements were made over a frequency band of 10 - 5000 cycles per second. The fluctuating component of wire voltage could be doubled by increasing the frequency band to 10,000 cycles per second. However, the major portion of the noise in the frequency range between 5,000 and 10,000 cycles was due to the wire support which was ringing at approximately 8,000 cycles. The audible ringing was verified with a microphone to be of the same frequency as that observed on the wire output voltage with a spectral analyzer.

A qualitative indication of the low turbulence level in the test section can be inferred from measurements which show that the boundary layer on the test section walls is laminar. This aspect is described in section 5.3.

CHAPTER 5

EVALUATION OF TUNNEL PERFORMANCE

5.1 Comparison of Wind Tunnel Performance with Predicted Performance

The design of the wind tunnel, and in particular the fan and motor selection, was based entirely on calculations described in Chapter 2. The reliability of these calculations is, therefore, an important consideration, since they can ultimately affect the wind tunnel performance. In addition to calibration and measurement of the turbulence level in the test section, measurements were made of various tunnel parameters and compared with predicted values.

5.2 Pressure Losses in the Effuser

The pressure losses in the stilling section and contraction section (effuser) were measured with total pressure rake (section 4.3) at the contraction section exit. The total pressure was measured relative to the ambient (test room) pressure and thus indicated the loss in total pressure. The predicted and measured pressure loss coefficient for the effuser is shown in figure 22. The results obtained agree with the predicted values for one test section dynamic pressure. The deviation of the pressure loss coefficient obtained experimentally from that predicted is probably due to variation of the screen pressure loss coefficient with velocity in the stilling section (see figure 3). This was not taken into account in the original calculations, since it represents a 2% change in the total tunnel pressure loss coefficient. In addition, the accuracy of the screen loss coefficient for a given mesh size is within the error introduced by omission of this effect.

5.3 Test Section Losses

The losses in the test section were obtained by measuring the static pressure along the test section walls. Assuming a laminar boundary growth along the test section walls, the calculated pressure losses are in very good agreement with the measured pressure losses (Figure 23). The test section taper, which was designed for a turbulent boundary layer growth, provides more expansion than is necessary for a laminar boundary layer growth. This is reflected by a decrease in dynamic pressure along the test section (see section 4.6). Using the exact methods for computing the pressure losses in laminar flow[11], one can obtain good agreement with results obtained with equation (2.16), provided an initial value of boundary layer thickness is assumed at the start of the test section.

5.4 Diffuser Performance

The primary consideration in the diffuser performance is the possibility of flow separation along its length, since this would incur additional pressure losses not accounted for in the calculations (section 2.4b). To indicate possible separation in the diffuser, static pressure taps were located along its length. Measurements of static pressure were made over the entire tunnel speed range with no evidence of separation along the diffuser. A typical diffuser recovery pressure plot is shown in figure 24, indicating no discontinuity in the curve.

Measurements of pressure losses in the diffuser were not made, since these are reflected in the total power required measurements and overall pressure losses for the circuit.

5.5 Fan Pressure Rise

The single parameter needed to obtain the power required and wind tunnel energy ratio is the fan static pressure rise, ΔP, as a function of mass flow through the test section.

Tables of fan characteristics were made available by the manufacturer from which the fan pressure rise could be obtained. The mass flow, measured at the test section and the fan speed where the two quantities necessary to determine the fan pressure rise. A plot of fan characteristics with the measured tunnel parameters is shown in figure 25. The fan pressure rise versus mass flow is shown in figure 26, and comparison with the predicted tunnel pressure losses from figure 10 shows excellent agreement for the zero blockage results.

5.6 Power Requirements

The power required for the tunnel can be obtained from a knowledge of the fan pressure rise and mass flow using equation (2.8). The required motor brake-horsepower is the power divided by the fan efficiency. The measured and calculated power requirements are shown in figure 27, again showing excellent agreement between the measured and predicted values.

5.7 Energy Ratio

The energy ratio as defined in equation (2.9) is a measure of tunnel efficiency. The measured and predicted values of energy ratio are shown in figure 28.

5.8 Fan Efficiency

The fan chosen for the tunnel was selected to provide operation of the tunnel near maximum fan efficiency. The fan characteristics for three selected mass flows are shown in figure 29, indicating the wind-tunnel operating point at these mass flows. As can be seen from this graph, the tunnel operates near the maximum fan efficiency over the entire range of tunnel speeds.

CHAPTER 6

CONCLUSIONS AND RECOMMENDATIONS

6.1 Summary of Wind Tunnel Design and Construction

An open circuit wind tunnel was designed and constructed for use with a magnetic suspension system. The goals in the design were to make a low cost, high efficiency wind tunnel with implementation of methods for reduction of turbulence in the test section. The selection of the fan and motor for the wind tunnel was based on calculations discussed in the text and chosen to provide fan operation near its maximum efficiency. A power supply for motor speed control was designed which provides continuous motor speed variations from ∿0 to 3000 r.p.m.

Calibration of the tunnel test section showed the maximum dynamic pressure to be 2.6 lb/in^2 for zero blockage at a maximum Reynolds number of 5×10^6 per foot and Mach number of 0.55.

Measurements were made to compare tunnel operating characteristics with calculations and found these to be in excellent agreement. The fan operates at maximum efficiency over the entire tunnel speed range.

The tunnel energy ratio was predicted by calculations and measured to be approximately 6.0 at half maximum speed (230 ft/sec).

The test section turbulence level was measured with a hot-wire and found to be less than 0.26% for freestream Reynolds numbers below 1.9×10^6 per foot. The test section velocity for this level of turbulence was 300 feet per second.

The methods for calculating pressure losses and power requirements for subsonic wind tunnels are outlined, and comparison with measurements show them to be in excellent agreement.

6.2 Wind Tunnel Operation with a Magnetic Suspension System

The primary purpose of this wind tunnel was to provide low cost operational experience and aerodynamic data with a magnetic suspension system. The wind tunnel has thus far proved to be operationally reliable and simple to operate. A substantial amount of aerodynamic data has been obtained with this tunnel and magnetic suspension system for which it was designed, the results of which are published in the literature[12,13].

APPENDIX A

A.1 Hot Wire Construction

The hot-wire probe used for measuring the turbulence level in the test section was made with a 0.125 diameter hypodermic tubing. The support prongs for the wire were made from needles epoxied to the probe and spread approximately 0.188 inches apart. The wire itself was 0.00012 in. diameter tungsten wire. The wire was copper plated at the ends, leaving approximately 0.080 in. of unplated wire in the middle. The plated ends were then soldered to the support prongs. The support prongs were electrically connected to two wires which were fed through static pressure taps in the tunnel wall. The probe itself was mounted on a stand attached to the tunnel walls.

A.2 Instrumentation

A constant current hot-wire anemometer system manufactured by Shapiro and Edwards (Model 50) was used with the hot-wire. The system consists of an amplifier for the wire output and contains the following items.

i.) Current Control Panel - provides current to the hot-wire as well as switching circuitry for the other components of the system.

ii.) Bridge and Potentiometer Circuits - used to measure the mean wire resistance, voltage and current.

iii.) Mean-Square Meter (thermocouple type) - measures the mean-square voltage fluctuations across the hot-wire.

iv.) Square-Wave Generator - used for calibrating the mean square-meter output as well as to set the compensation for the hot wire (due to its thermal inertia).

A.3 Hot-Wire Calibration

For a given hot-wire the relation between the wire resistance, R, and velocity over the wire, V, has been shown[14] to be of the form

$$\frac{i^2 R}{R - R_g} = A + B\sqrt{V} \qquad (A.1)$$

where i is the wire current and Rg is the wire "cold" resistance or unheated resistance. The constants A and B can be determined for a given wire by measuring the flow velocity and the wire resistance at constant current. The calibration curve for the wire used is shown in figure A-1 at two different heating currents. The slope of each curve gives the value of B from equation (A.1).

A.4 Hot-Wire Response to Velocity Fluctuations

Using equation (A.1) for steady flow and substituting $R = \bar{R} + r$ and $V = \bar{V} + v$, where r and v are fluctuations with zero mean value one obtains

$$\frac{i^2(\bar{R} + r)}{\bar{R} + r - R_g} = A + B(\bar{V} + v)^{0.5} \qquad (A.2)$$

If the fluctuations in resistance are small compared to the mean value of the resistance ($r \ll \bar{R}$) equation (A.2) becomes

$$\frac{v}{\bar{V}} \cong \frac{i^2 R_g e}{0.5\,\bar{V}^{0.5}(R - R_g)^2} \qquad (A.3)$$

where e = ir.

The root-mean-square of the velocity $\sqrt{\overline{v^2}}$

$$\frac{\sqrt{\overline{v^2}}}{\bar{V}} = \frac{i^2 R_g \sqrt{\overline{e^2}}}{0.5\,B\bar{V}^{0.5}(R - R_g^2)} \qquad (A.4)$$

Measurement of the root-mean-square voltage fluctuation of the wire will give the root-mean square velocity fluctuation once the wire has been calibrated as described in section A.3.

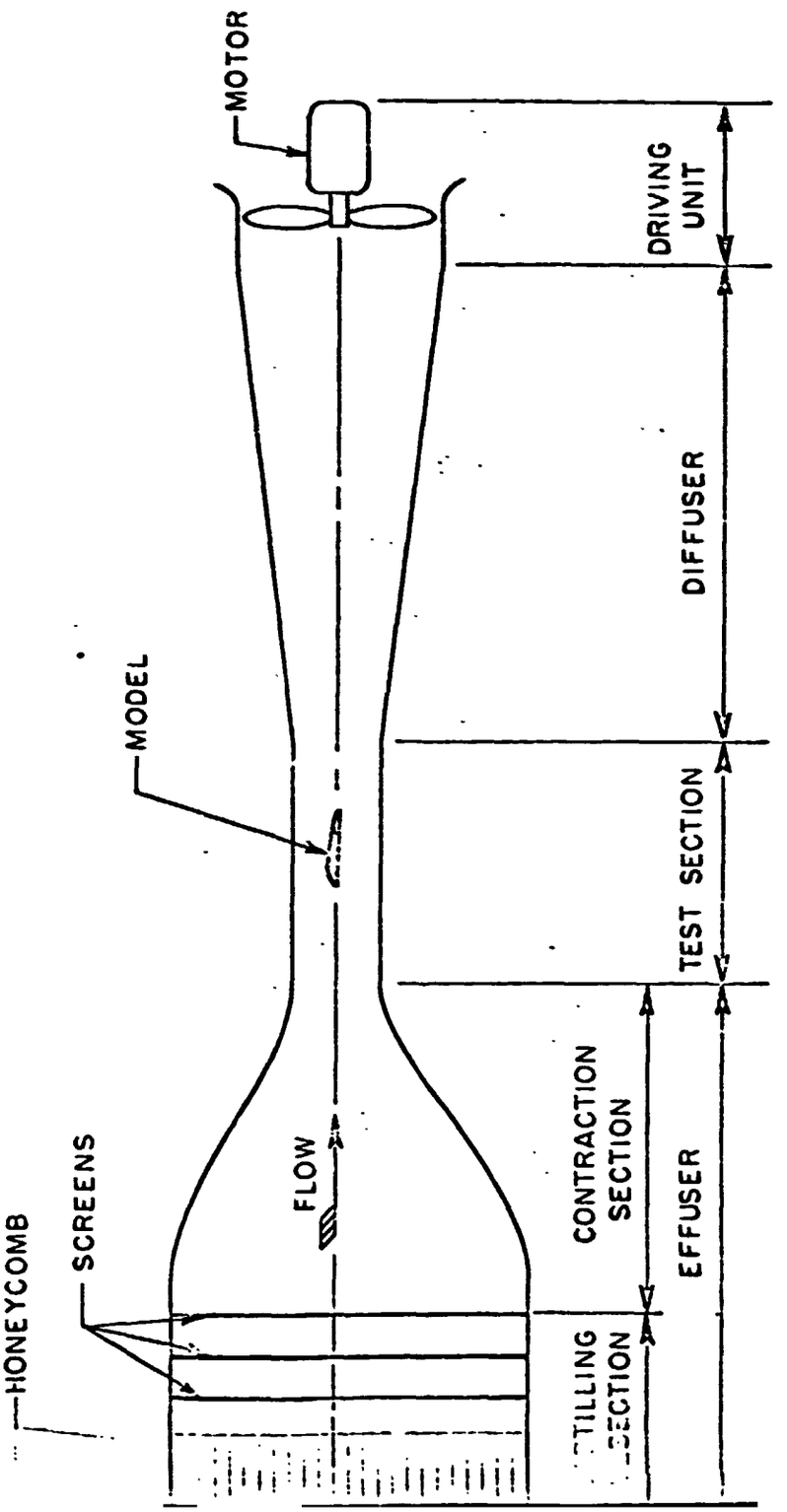

Figure 1. Open circuit tunnel configuration

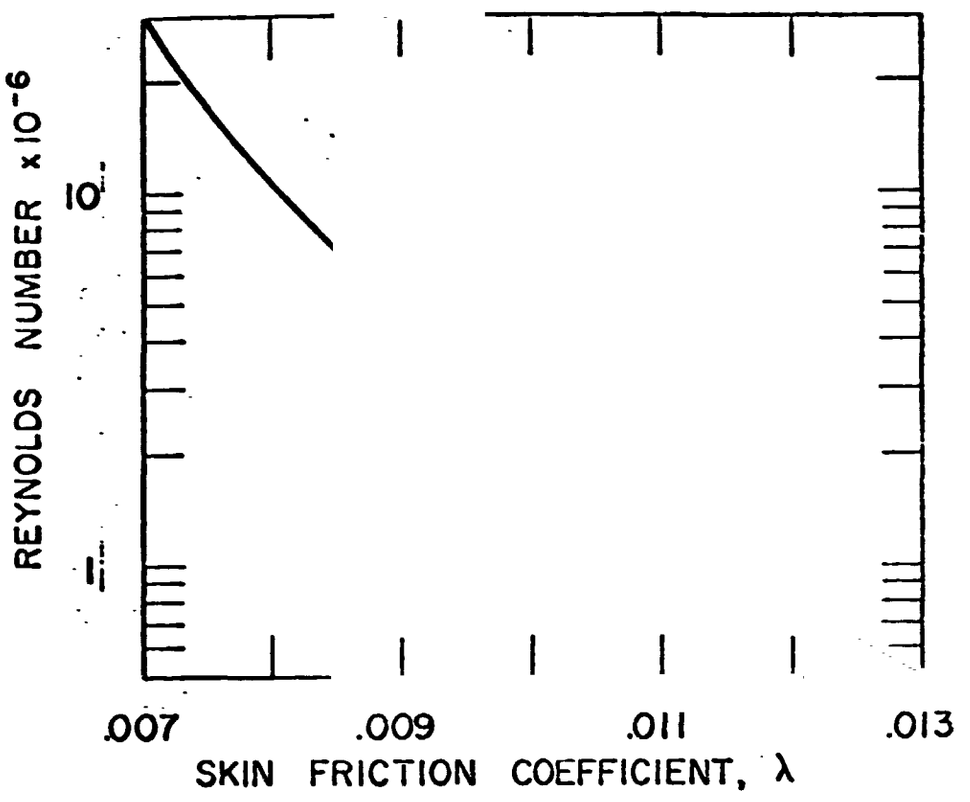

Figure 2. Friction coefficient versus Reynolds number (from Ref 2)

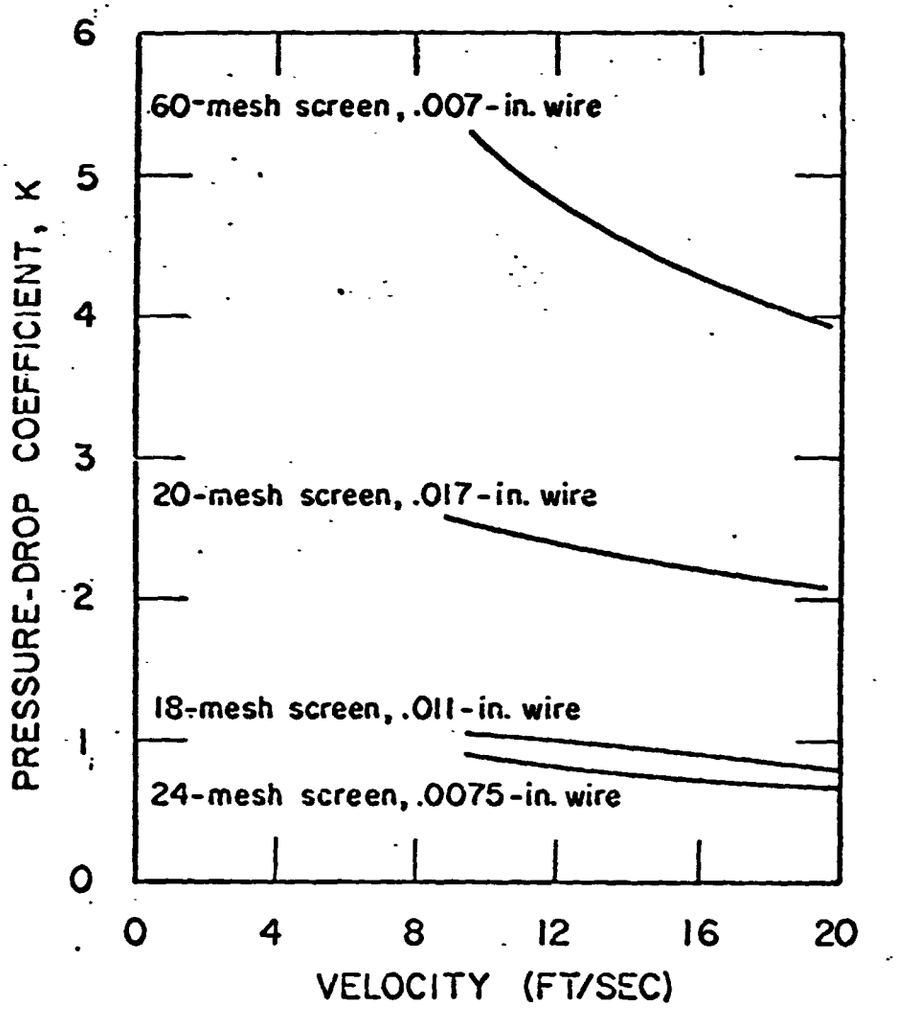

Figure 3. Pressure loss coefficient for screens (from Ref. 2)

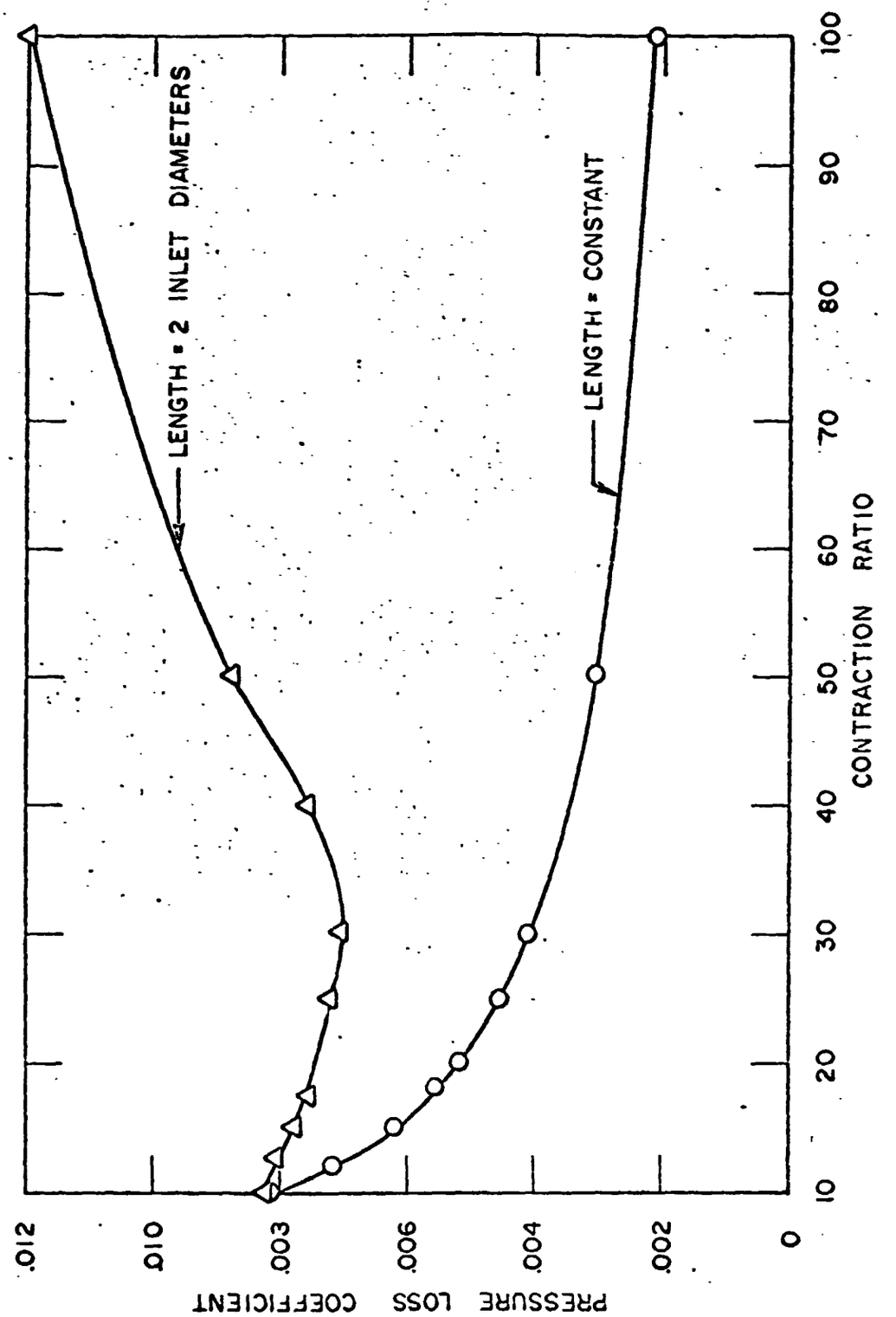

Figure 4. Contraction section losses for various contraction ratios

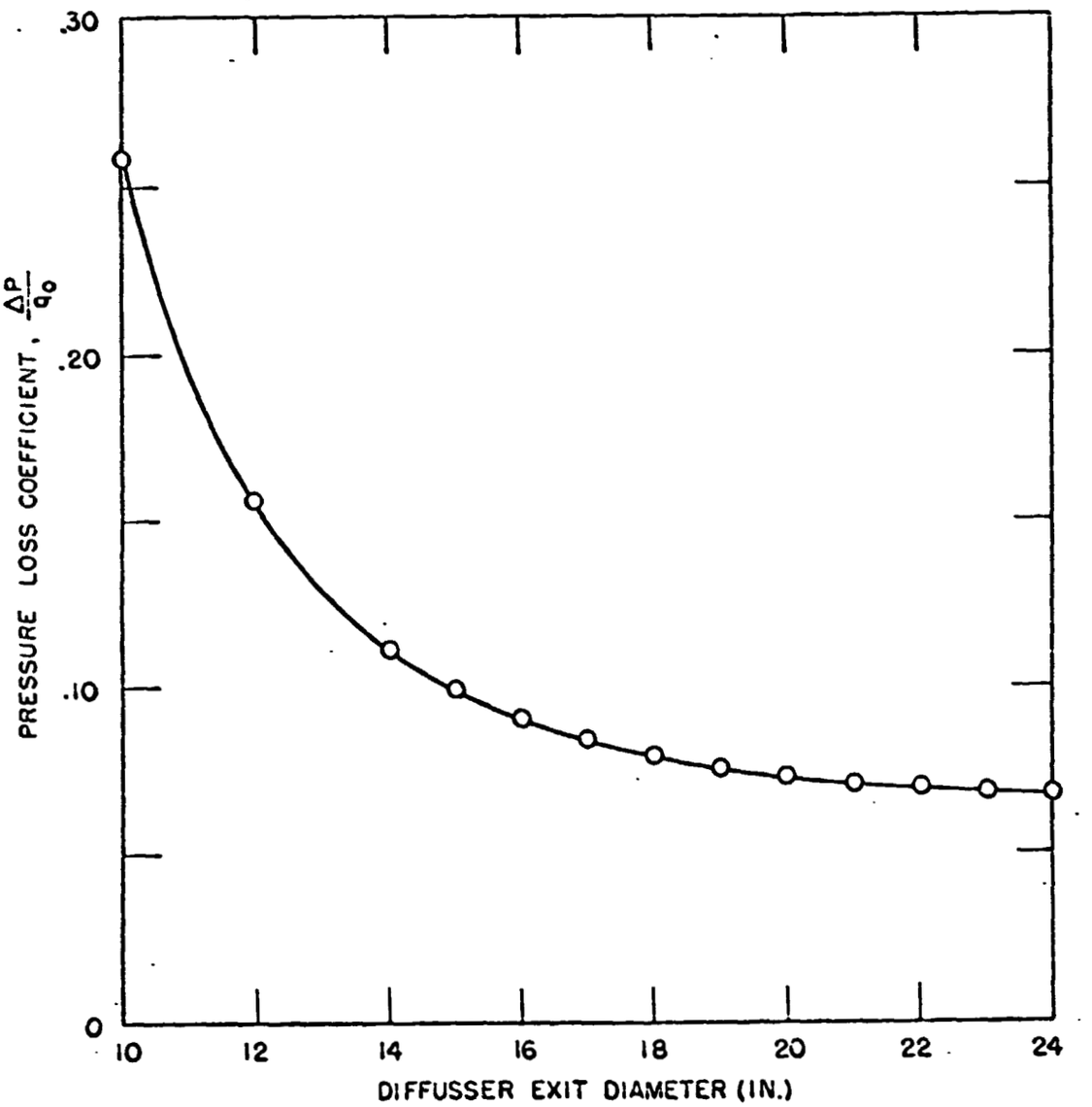

Figure 5. Diffuser losses for various exit diameters

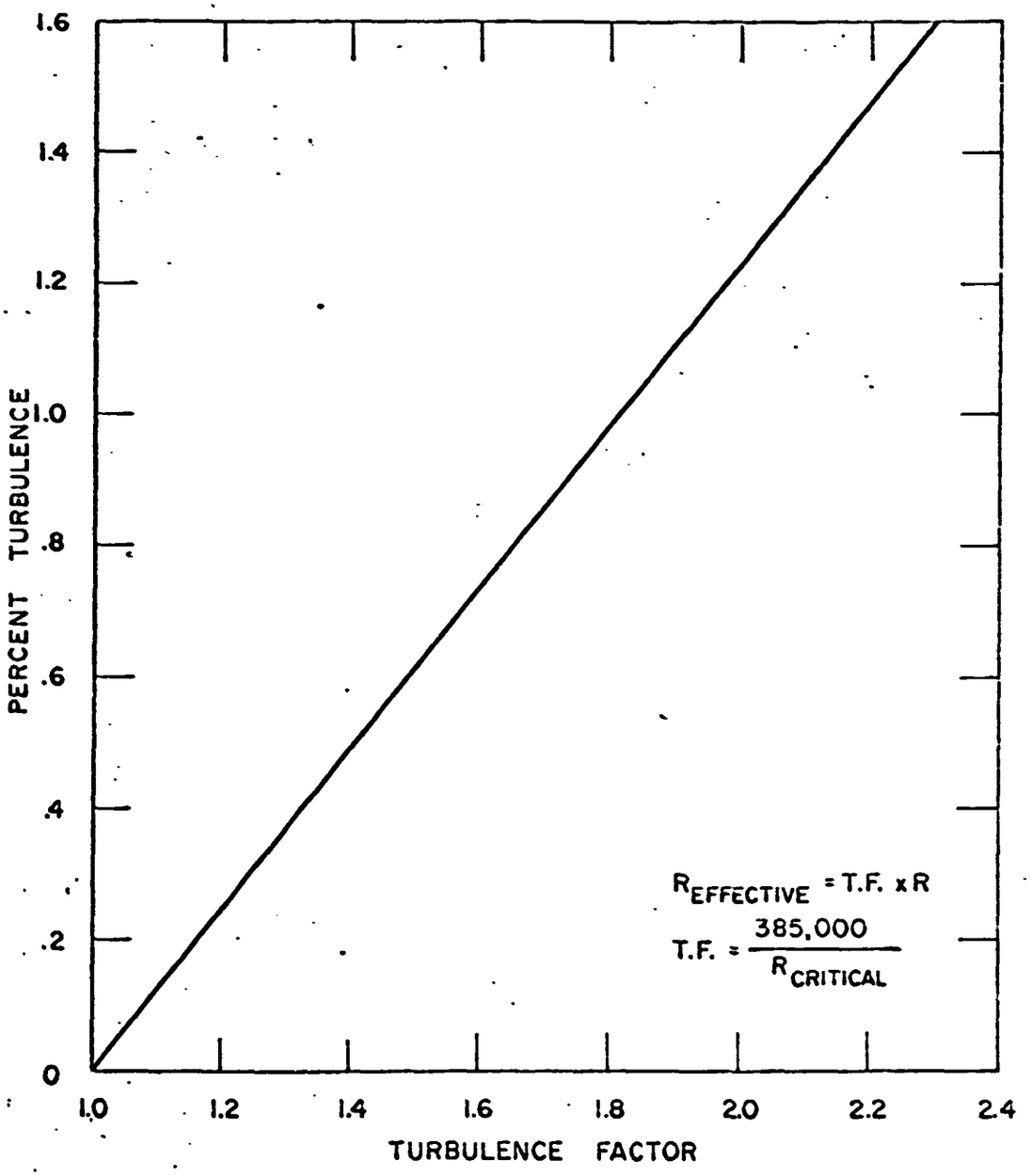

Figure 6. Turbulence factor versus turbulence level (from Ref 2)

Figure 7. Wind tunnel and magnetic balance

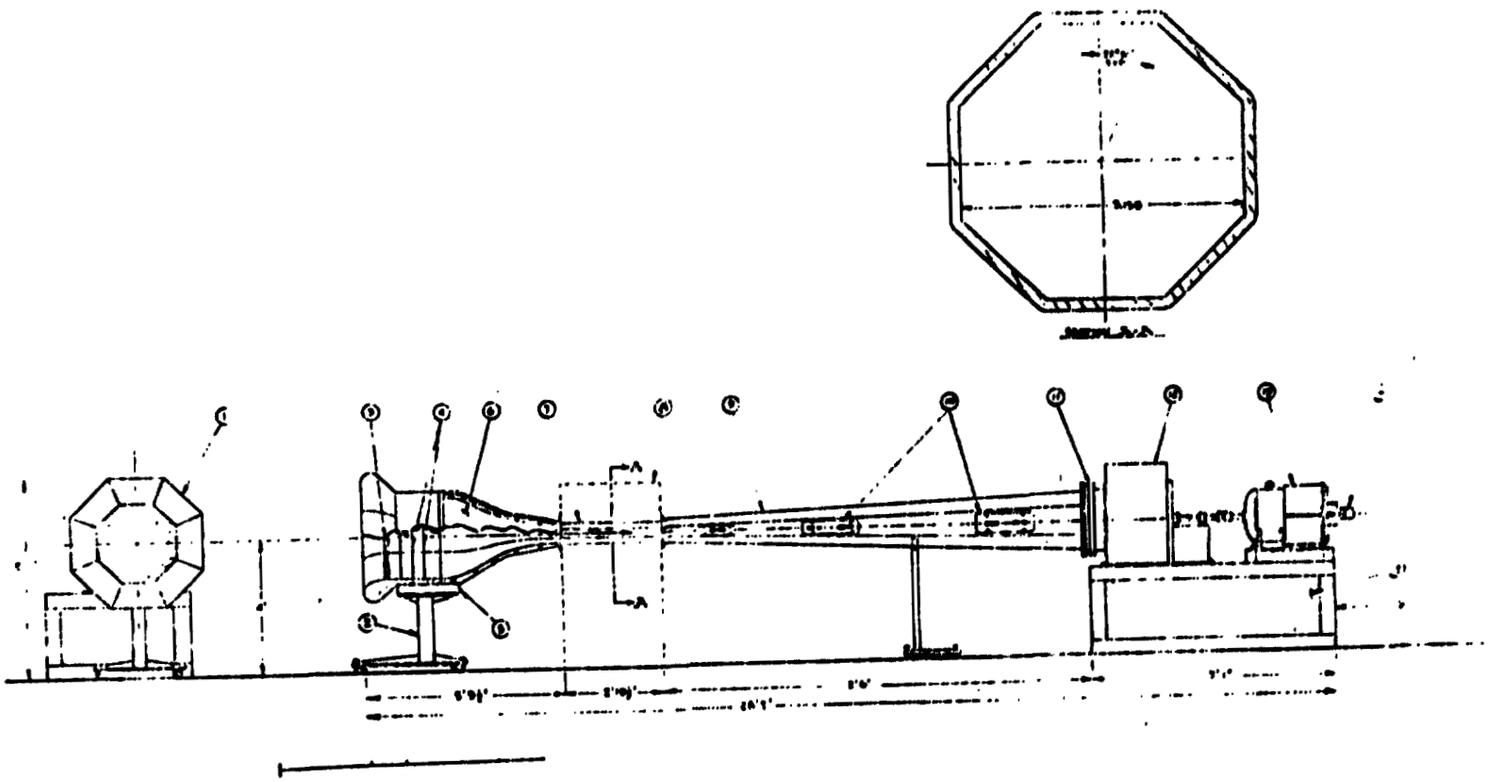

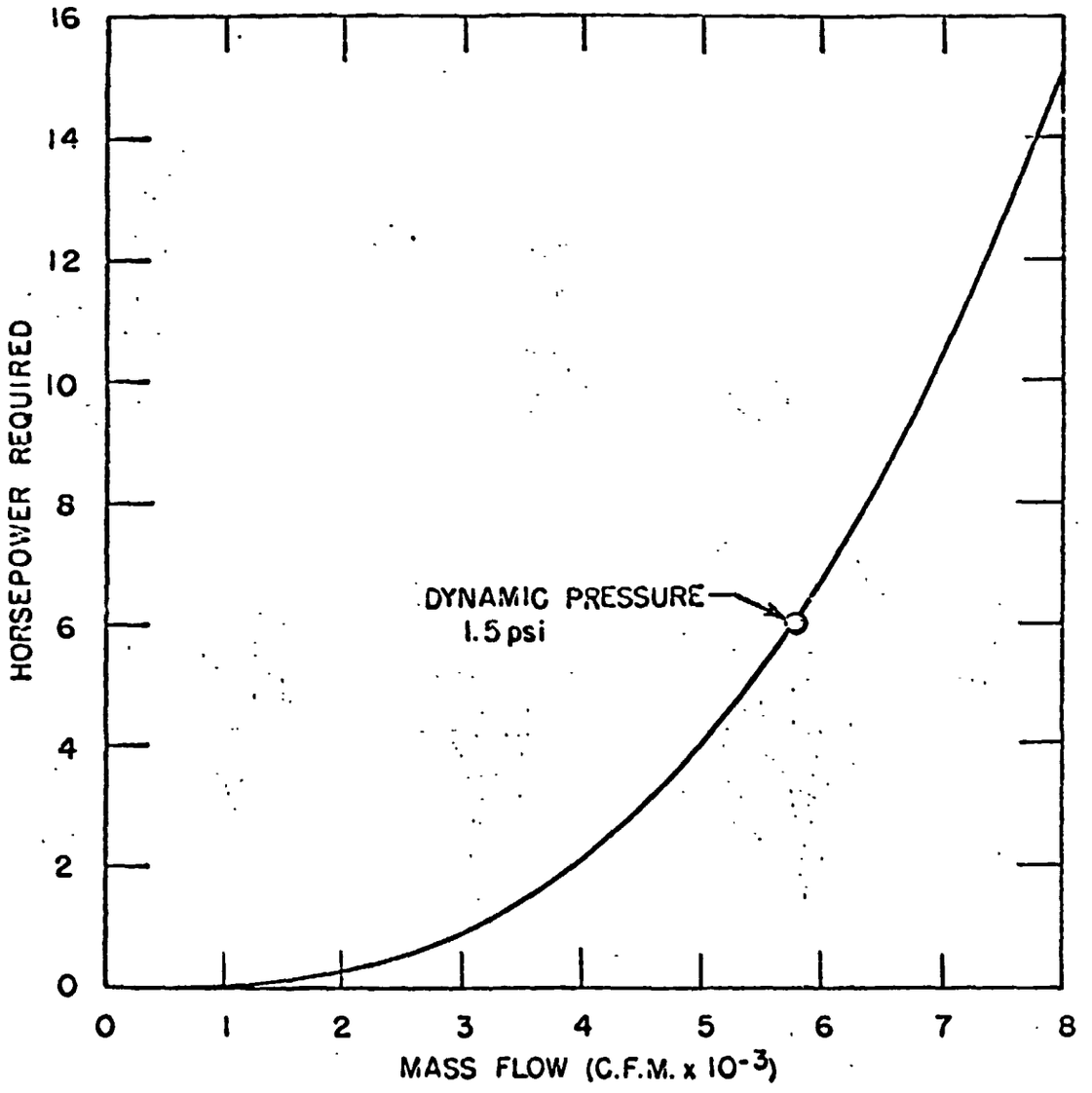

Figure 9. Required power versus mass flow rate

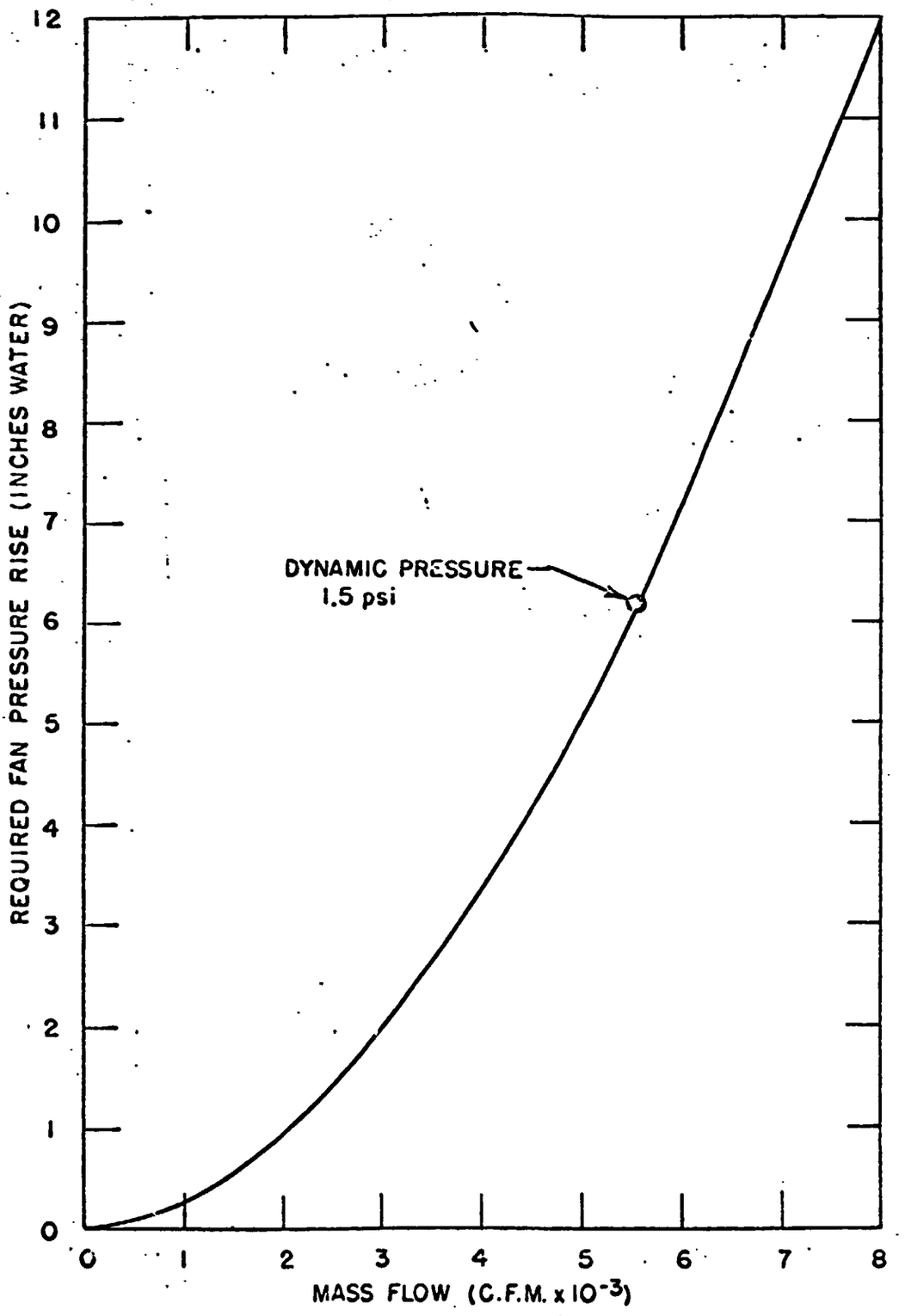

Figure 10. Required fan pressure rise versus mass flow rate

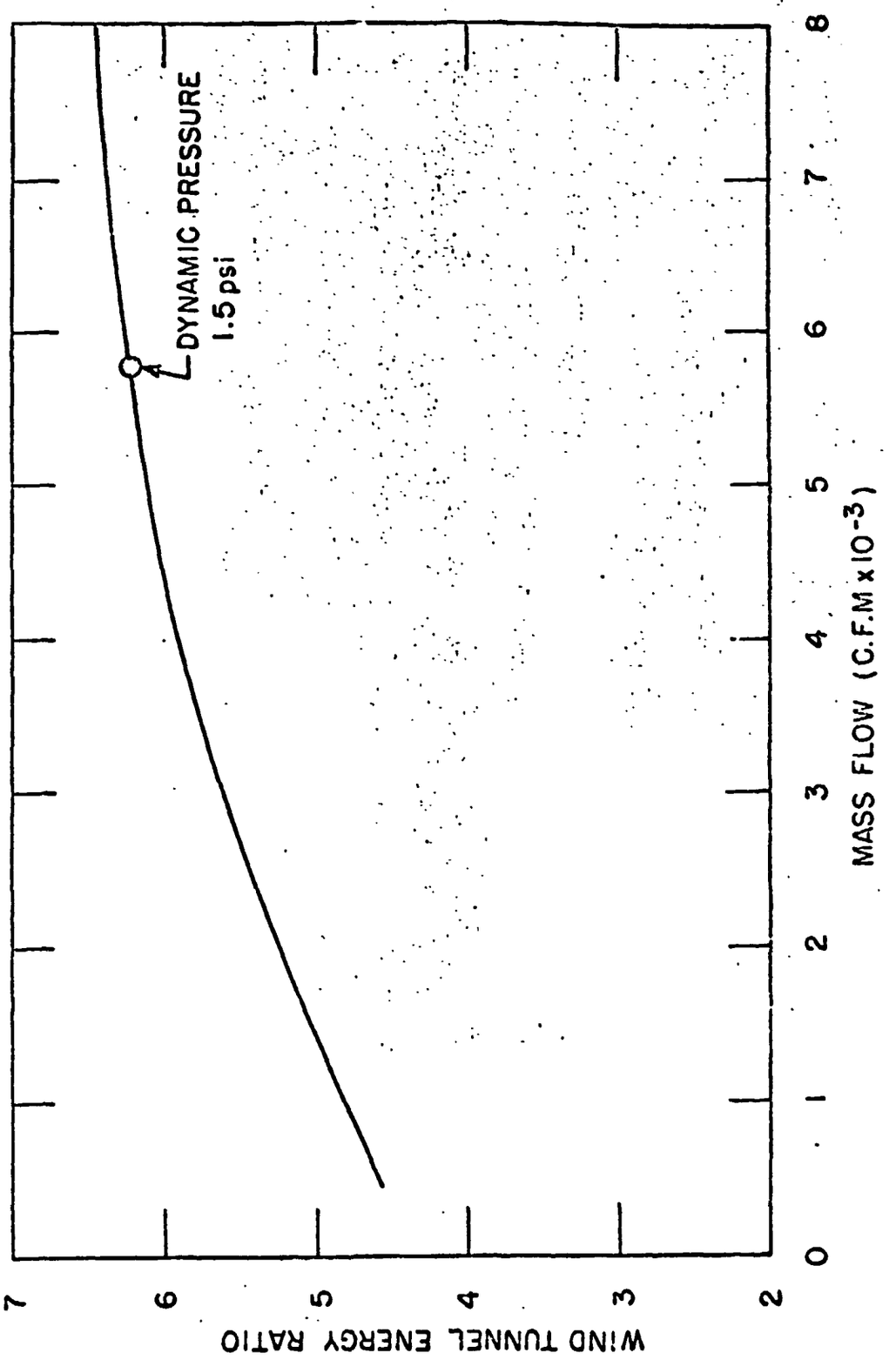

Figure 11. Tunnel energy ratio versus mass flow rate

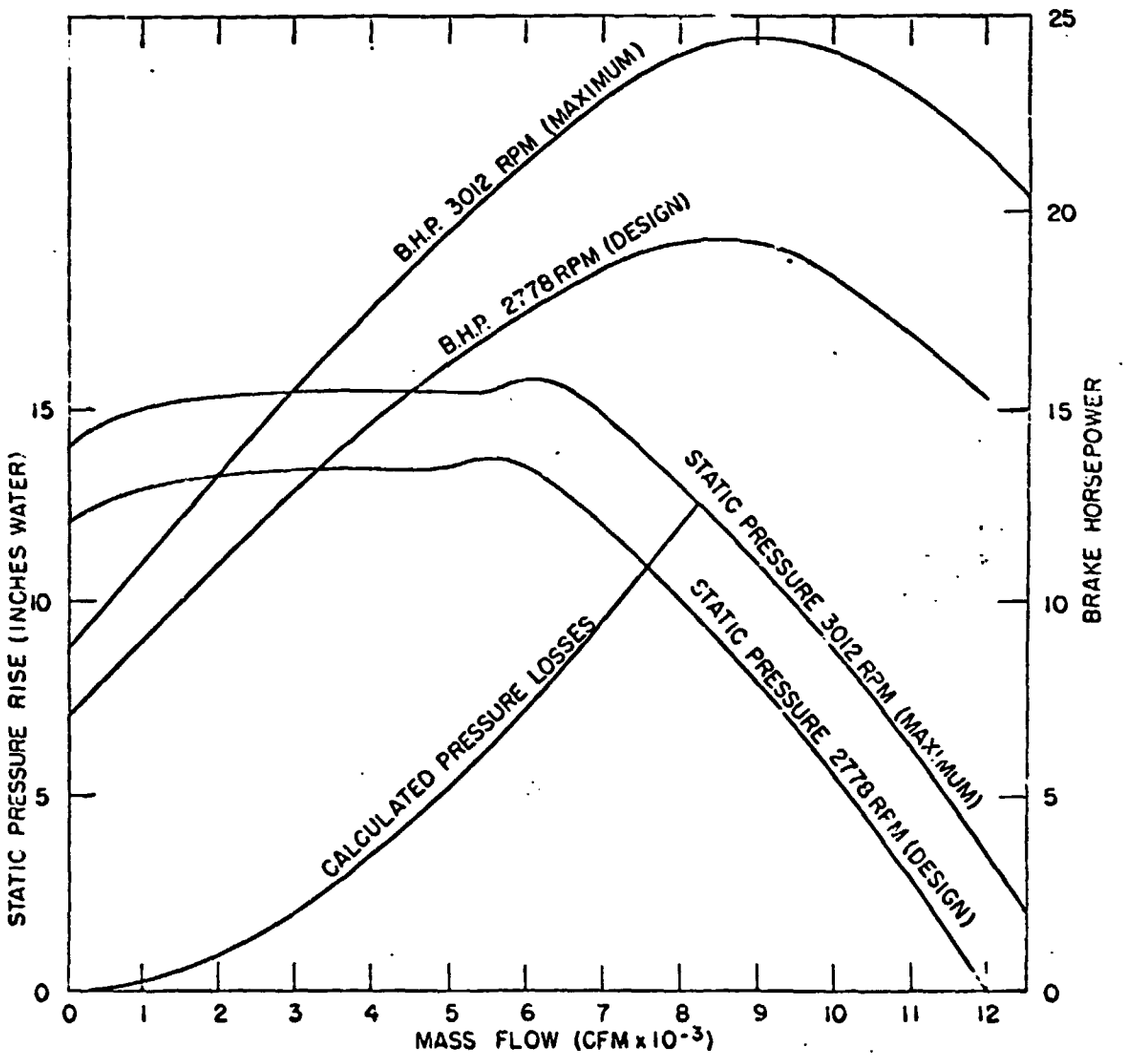

Figure 12. Fan operating characteristics and predicted tunnel requirements

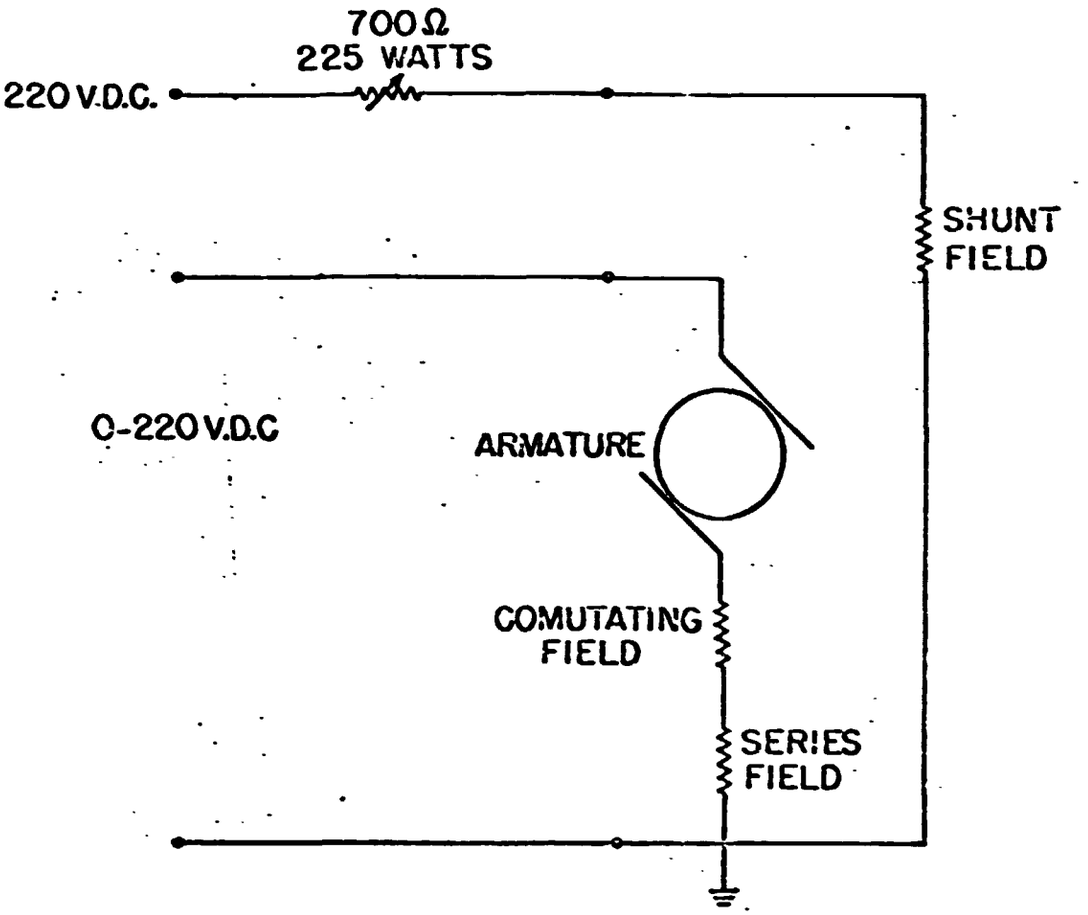

Figure 13. Motor windings schematic

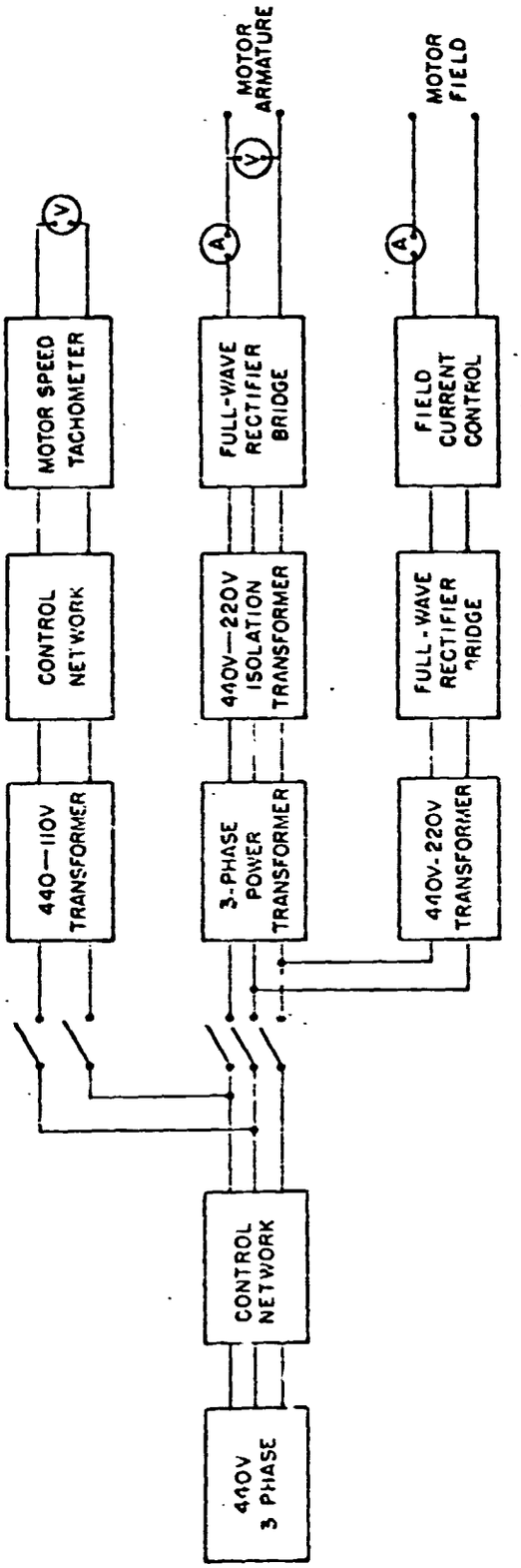

Figure 14. Power supply block diagram

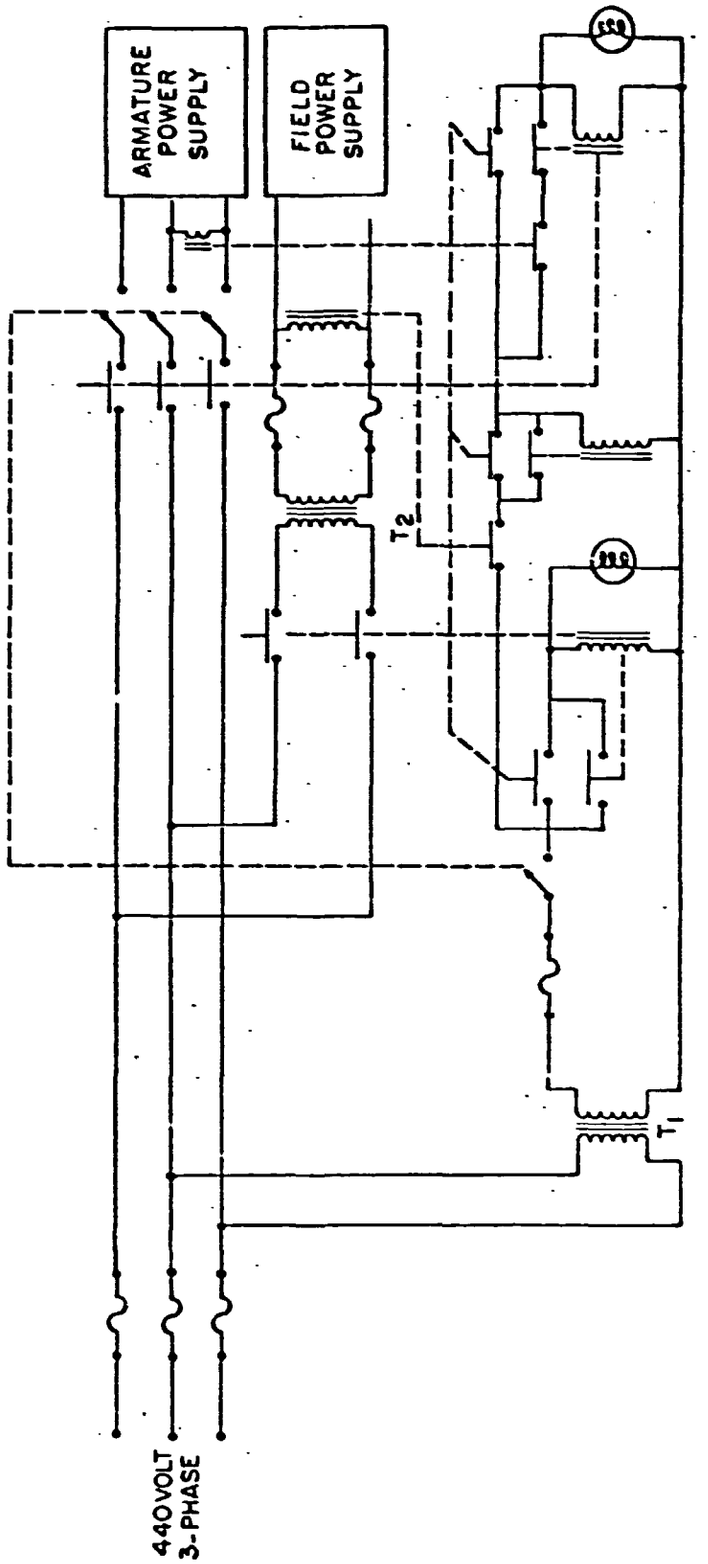

T_1 440/110 VOLT TRANSFORMER
T_2 440/220 VOLT TRANSFORMER

Figure 15. Control circuit schematic

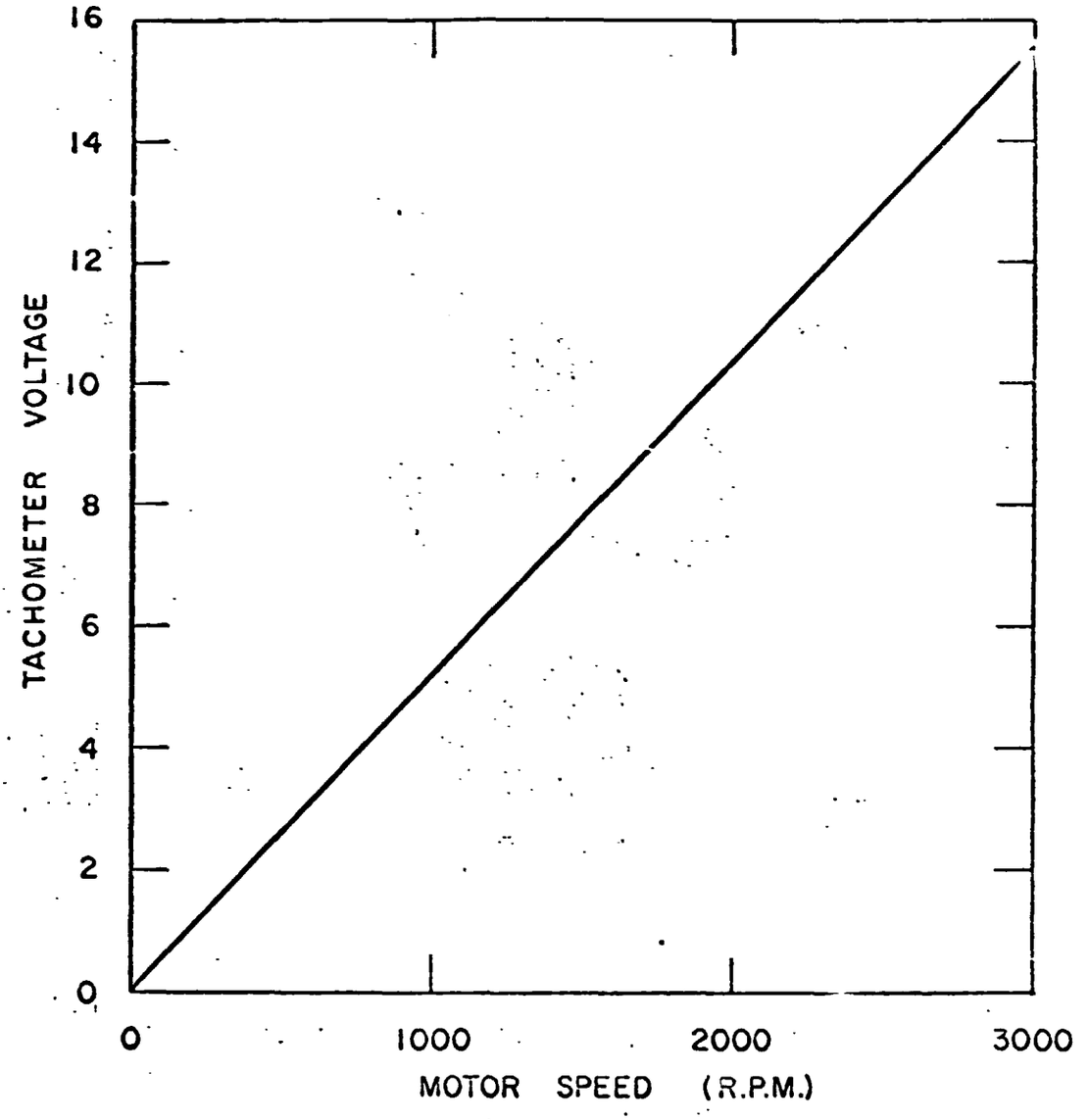

Figure 16. Motor speed versus tachometer voltage

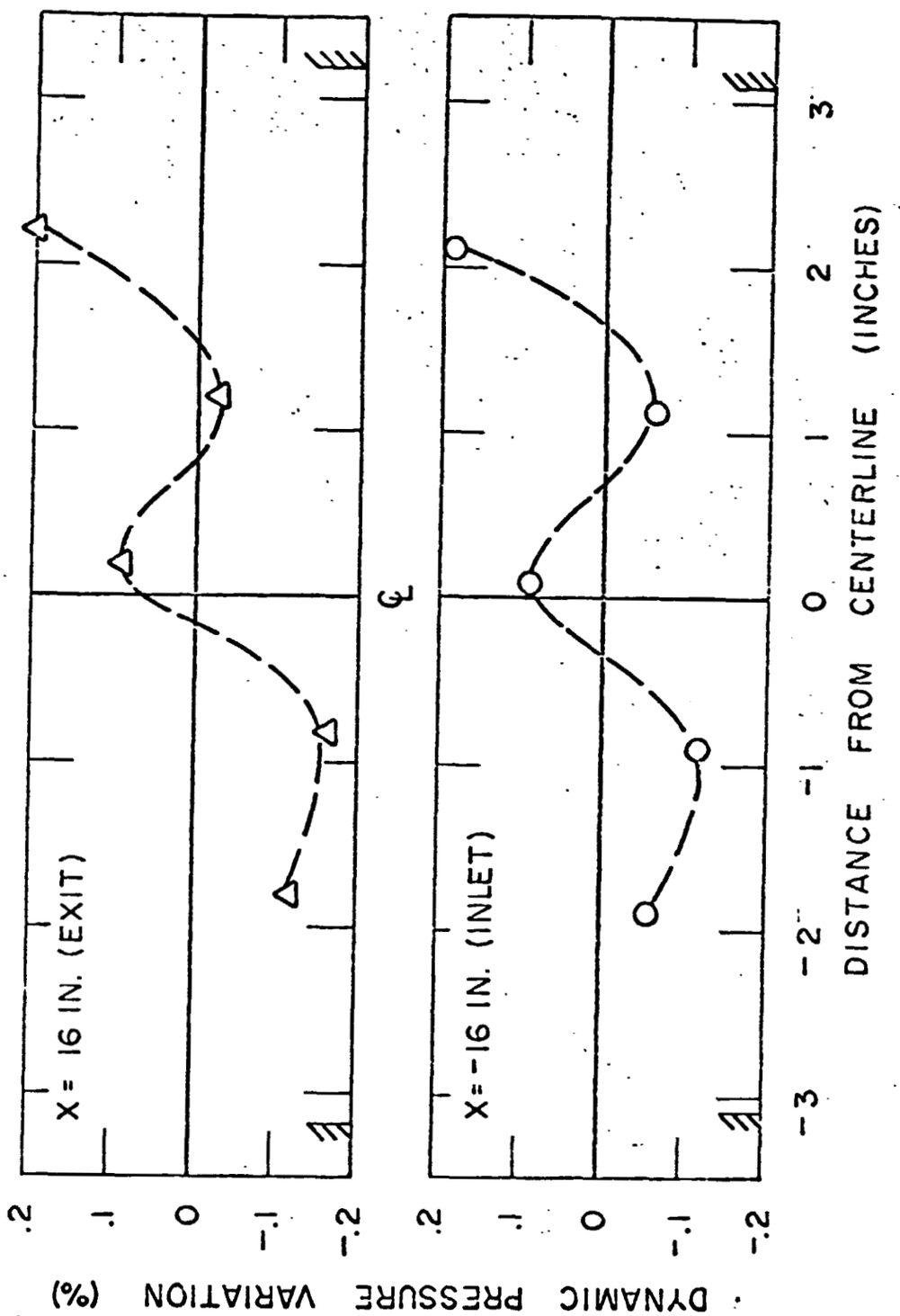

Figure 17. Spanwise test section dynamic pressure variation

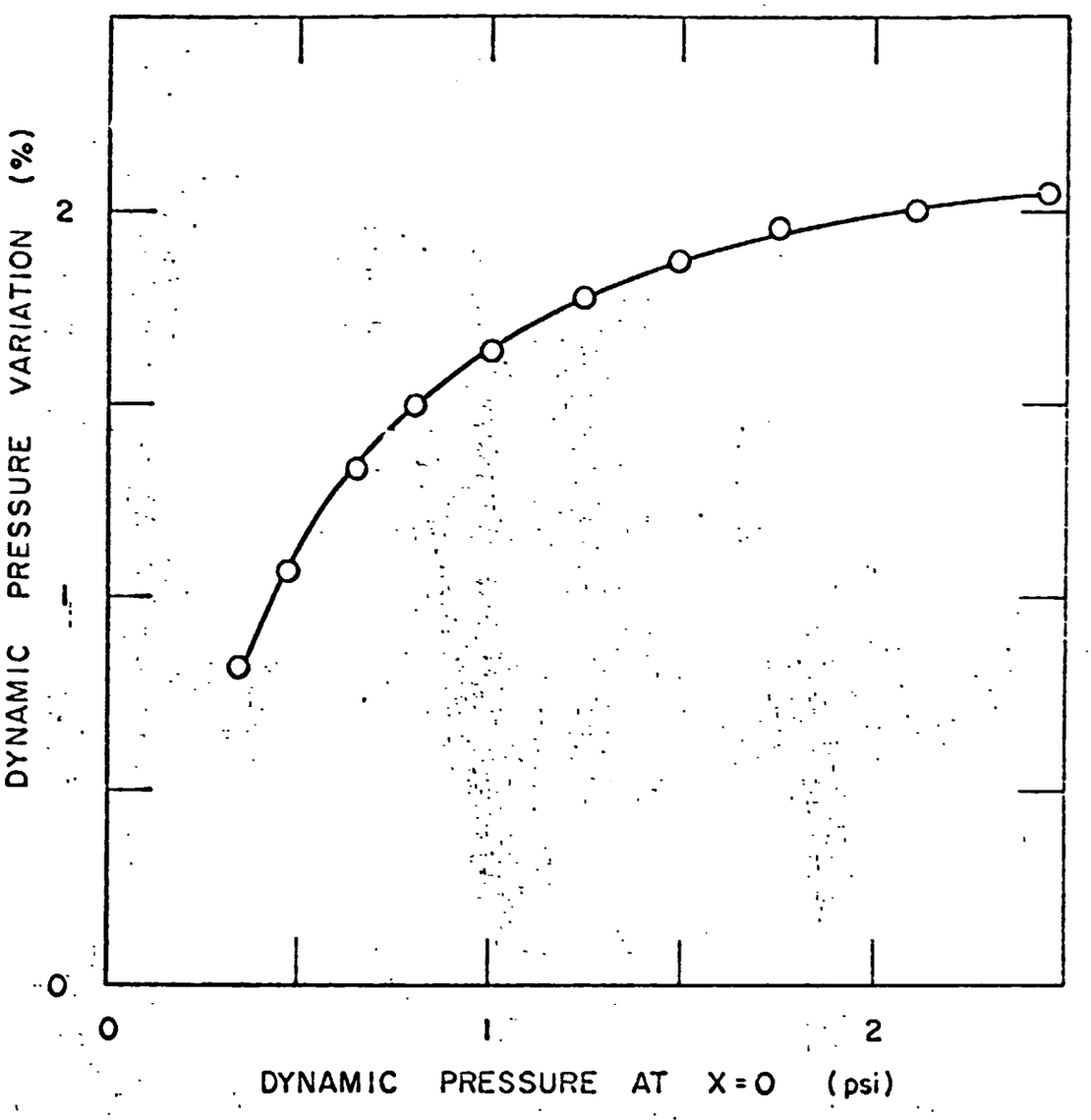

Figure 18. Dynamic pressure variation between inlet and exit versus centerline dynamic pressure

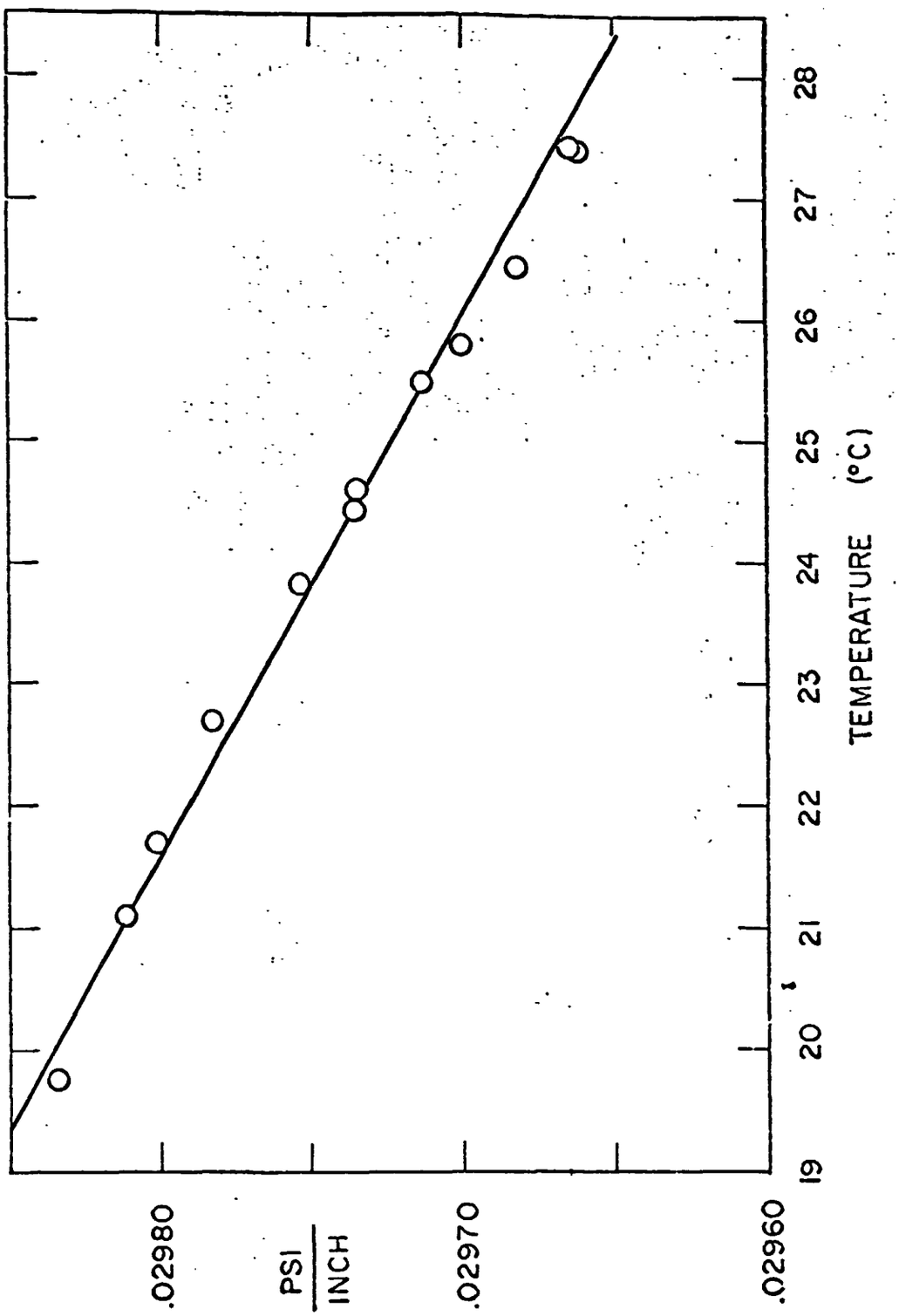

Figure 19. Speed setting manometer fluid density versus temperature

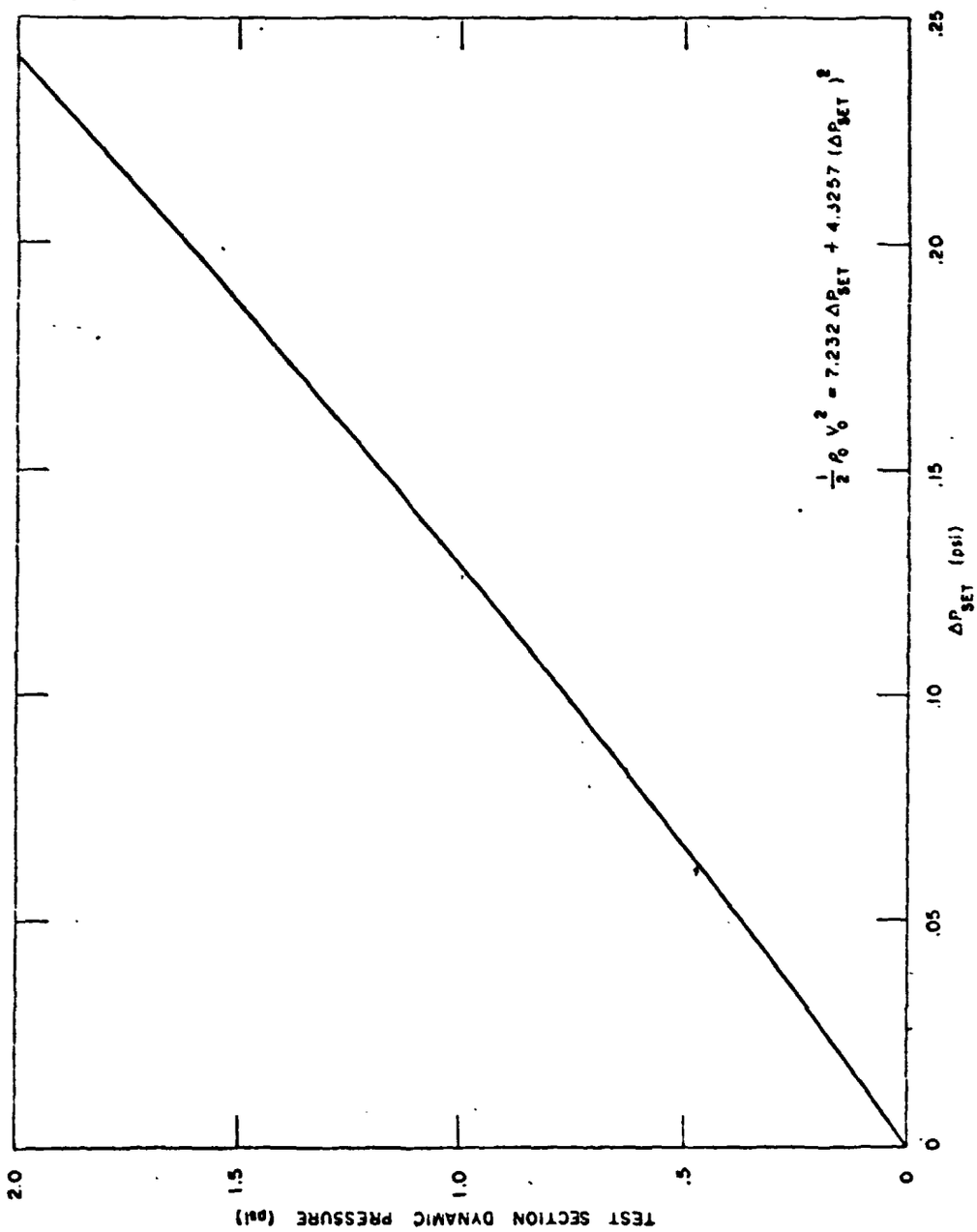

Figure 20. Test section dynamic pressure versus speed setting pressure

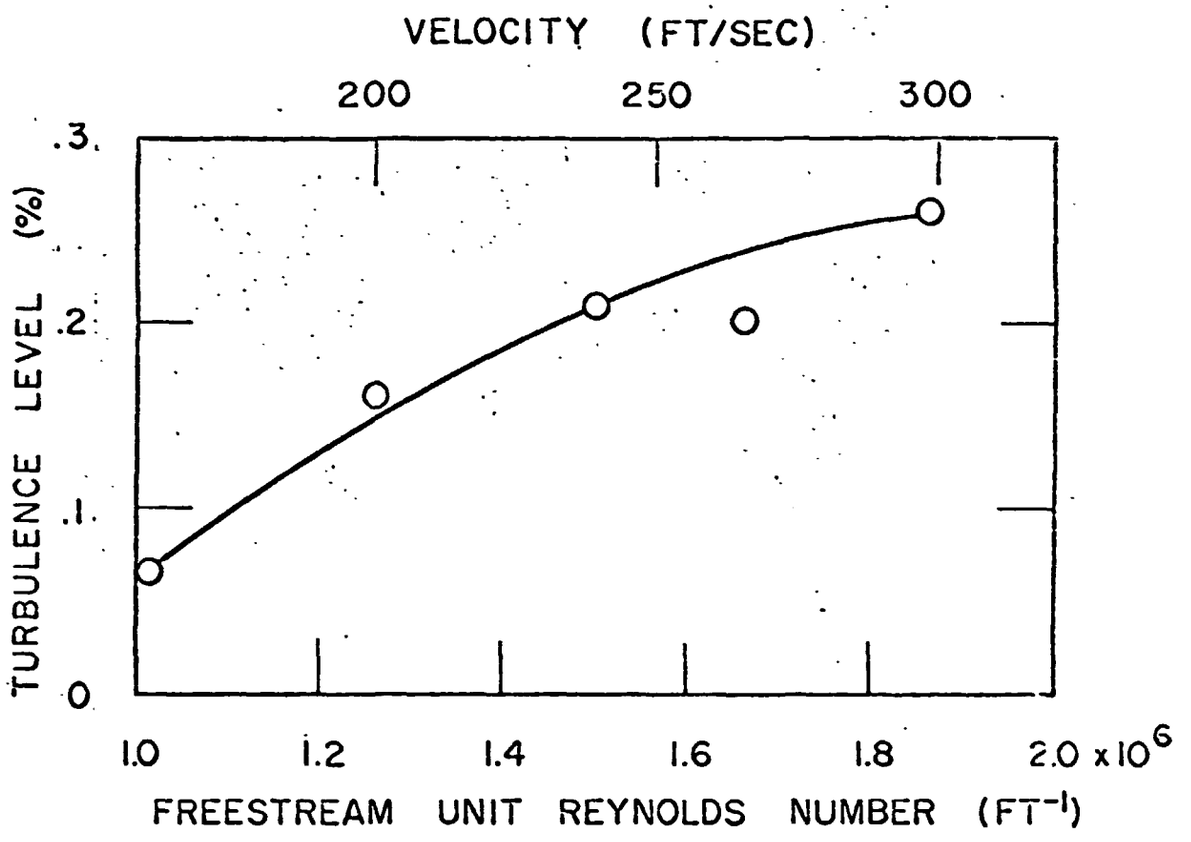

Figure 21. Test section turbulence versus Reynolds number and velocity

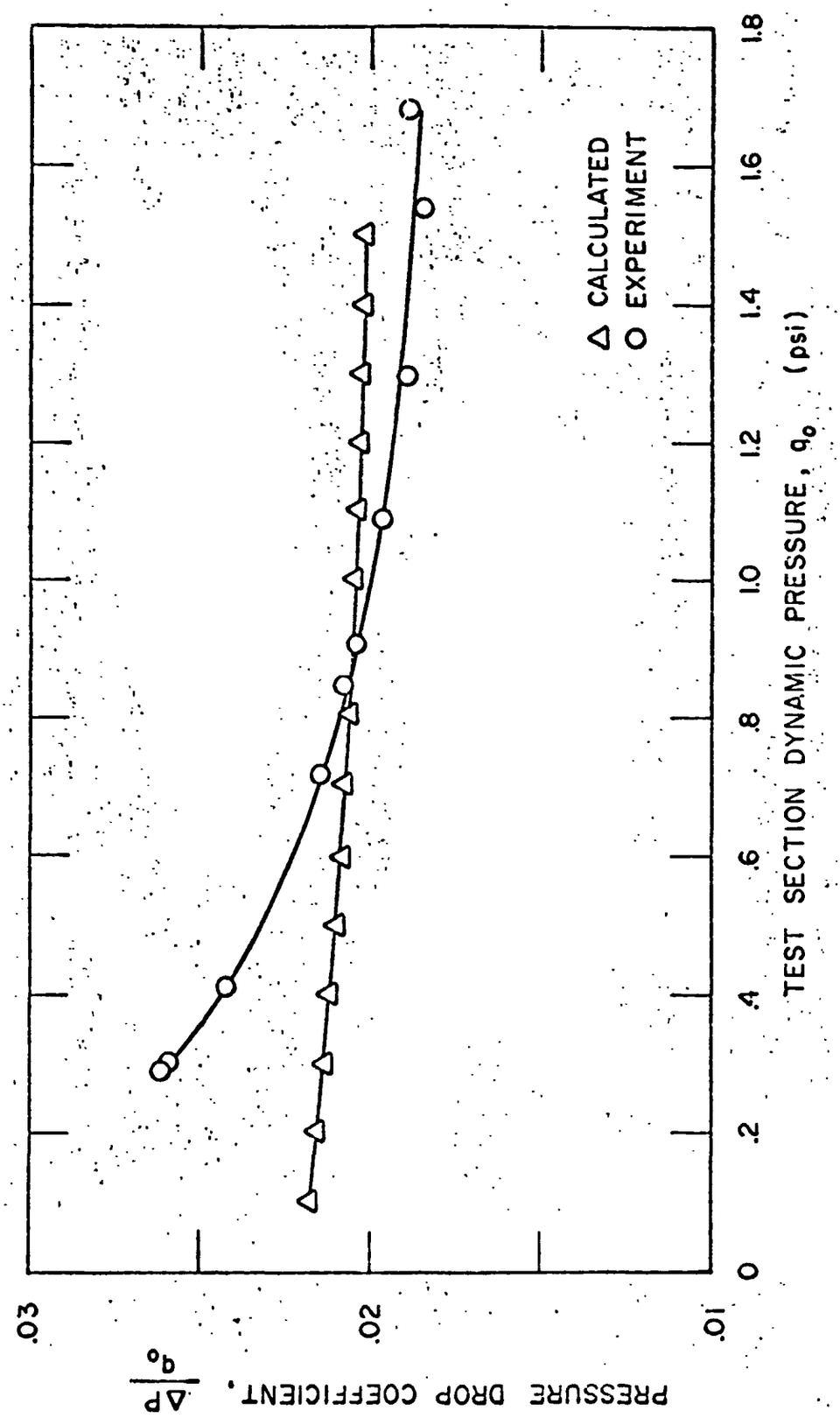

Figure 22. Effuser pressure loss coefficient versus test section dynamic pressure

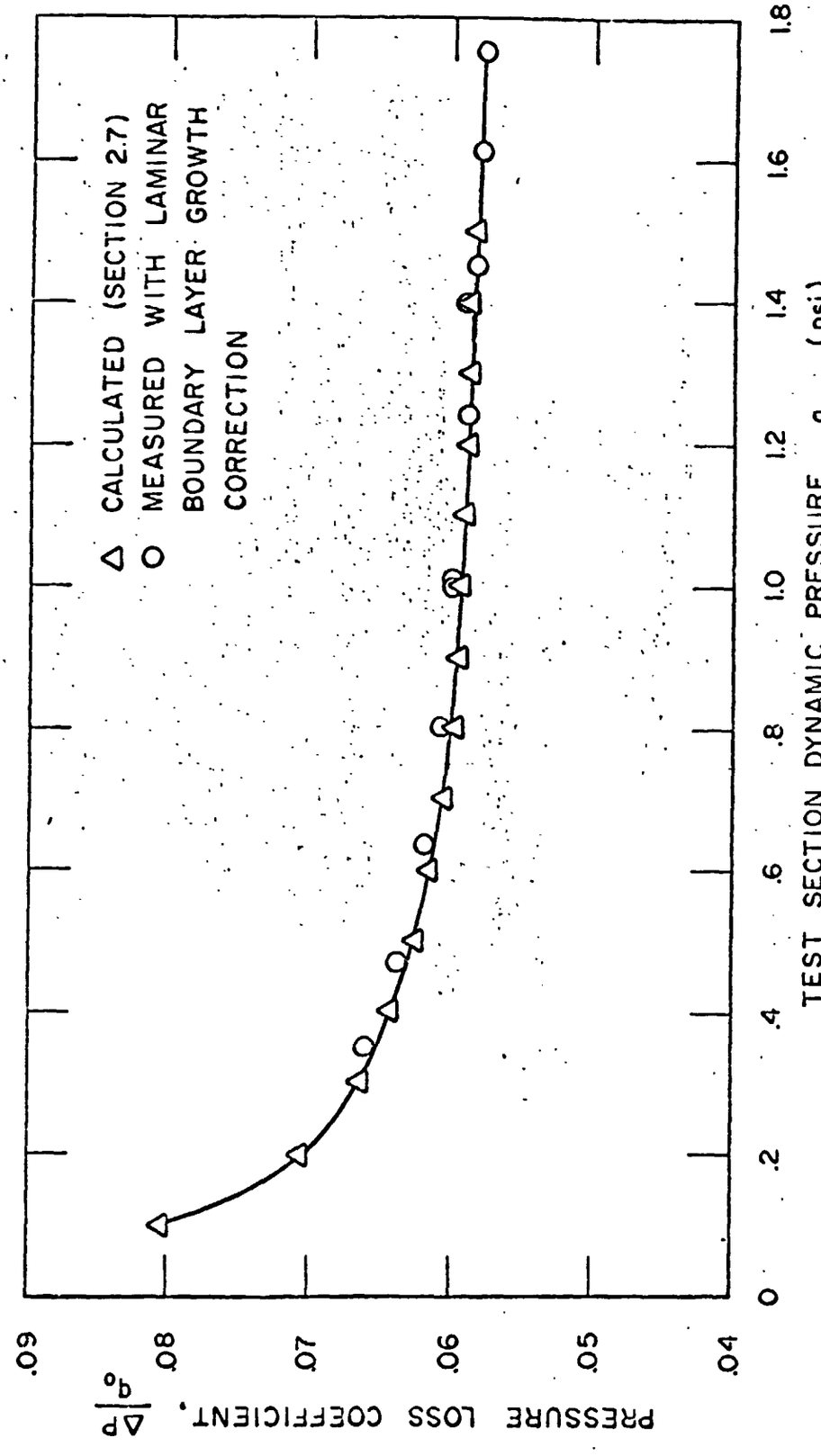

Figure 23. Test section pressure loss coefficient versus dynamic pressure

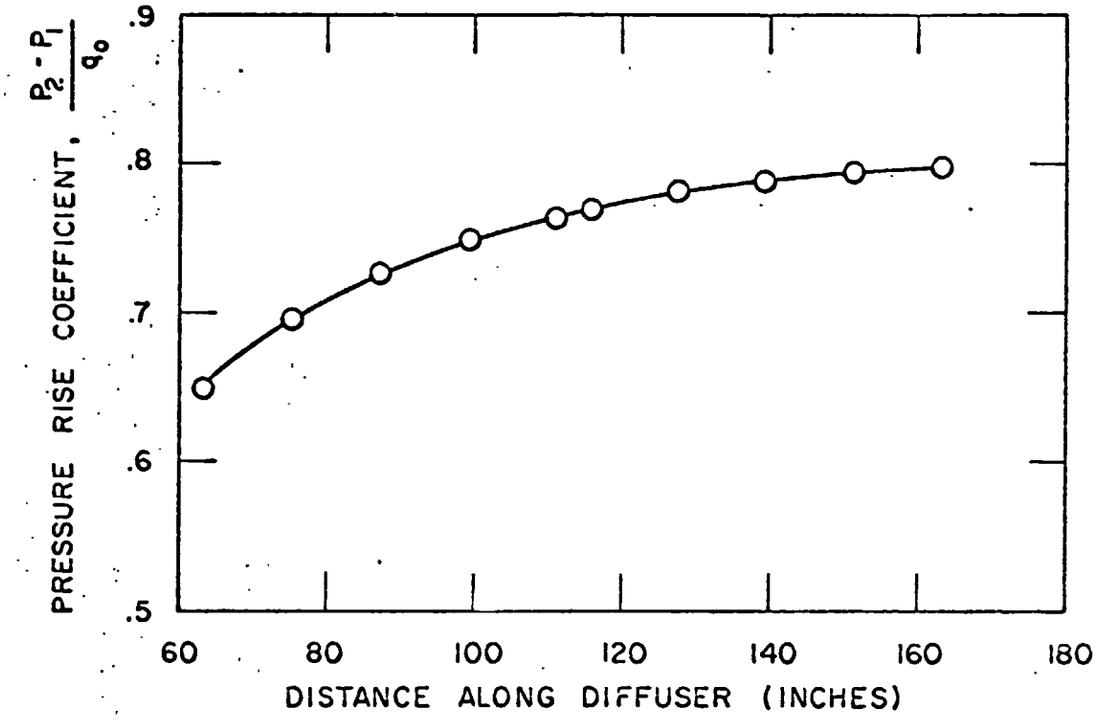

Figure 24. Diffuser pressure recovery

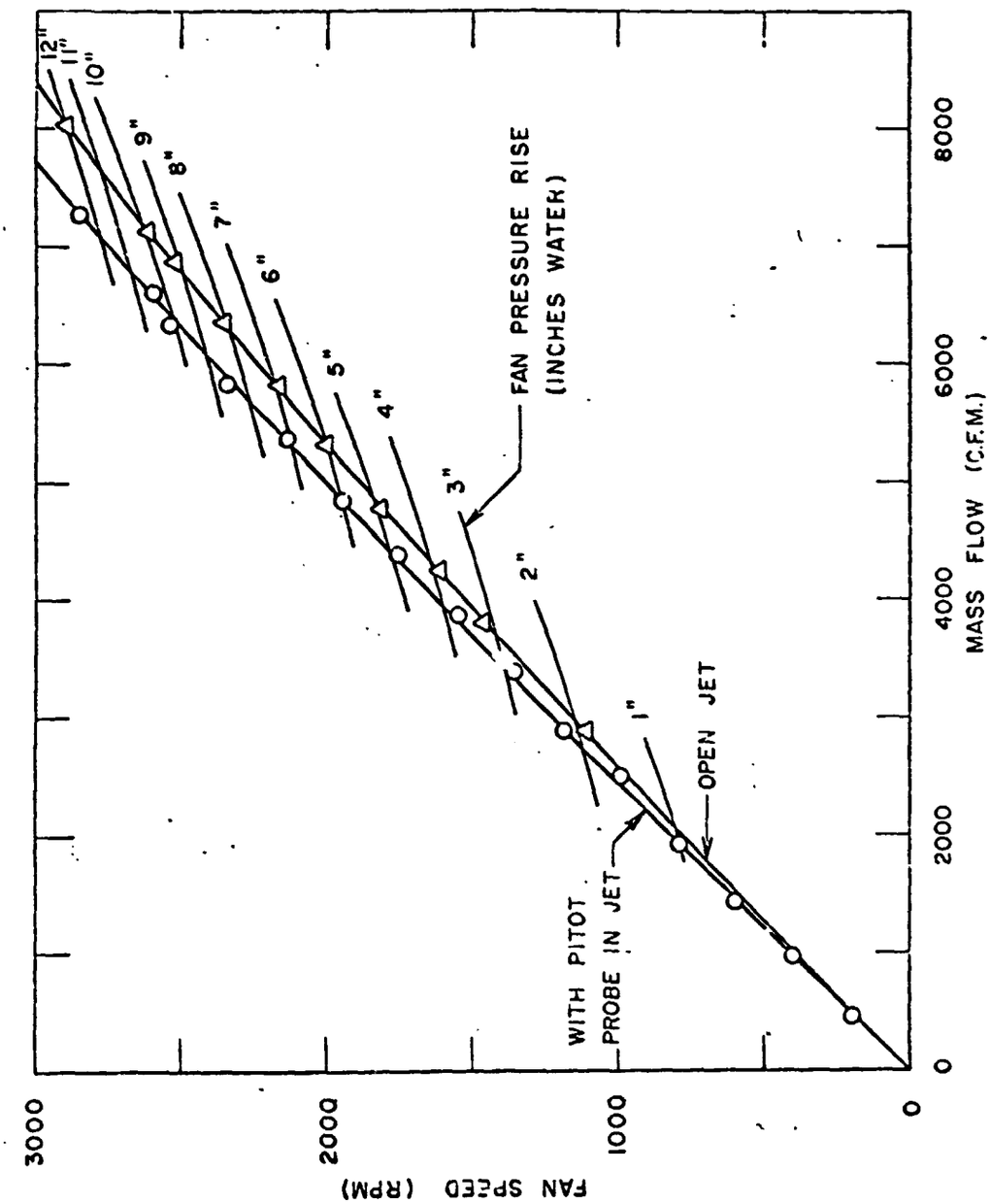

Figure 25. Fan characteristics and measured wind tunnel requirements

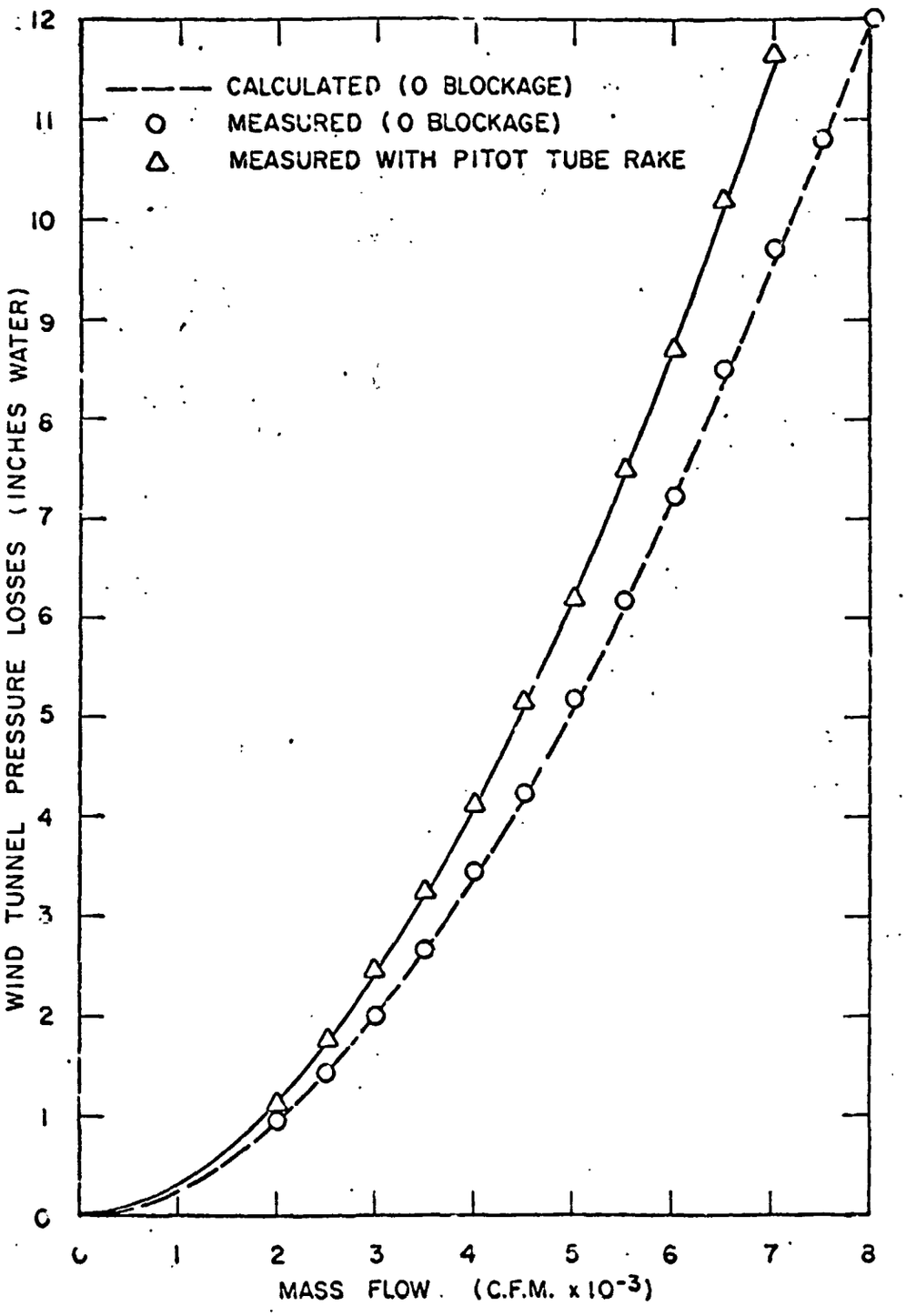

Figure 26. Wind tunnel pressure rise versus mass flow

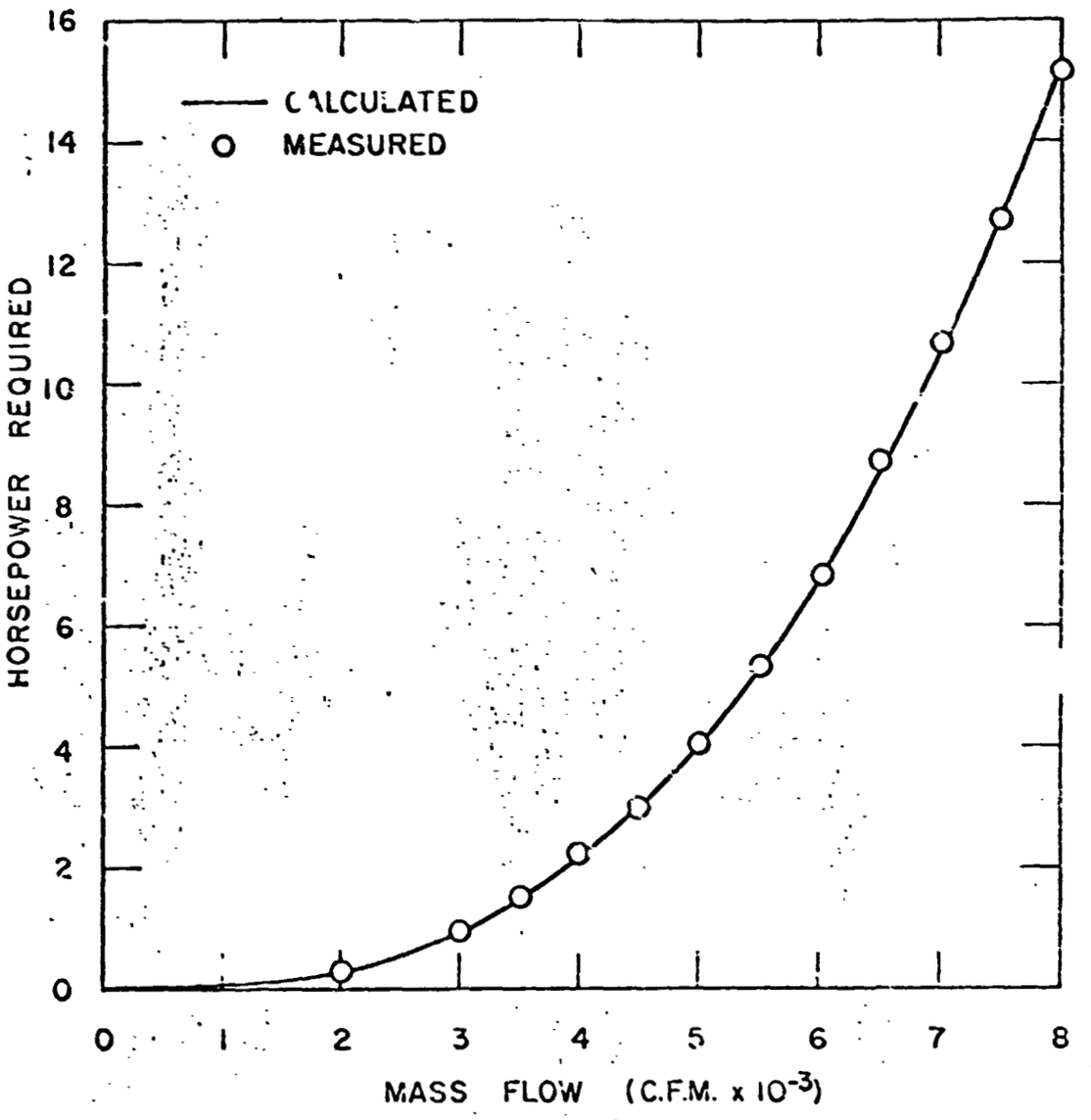

Figure 27. Measured power required versus mass flow

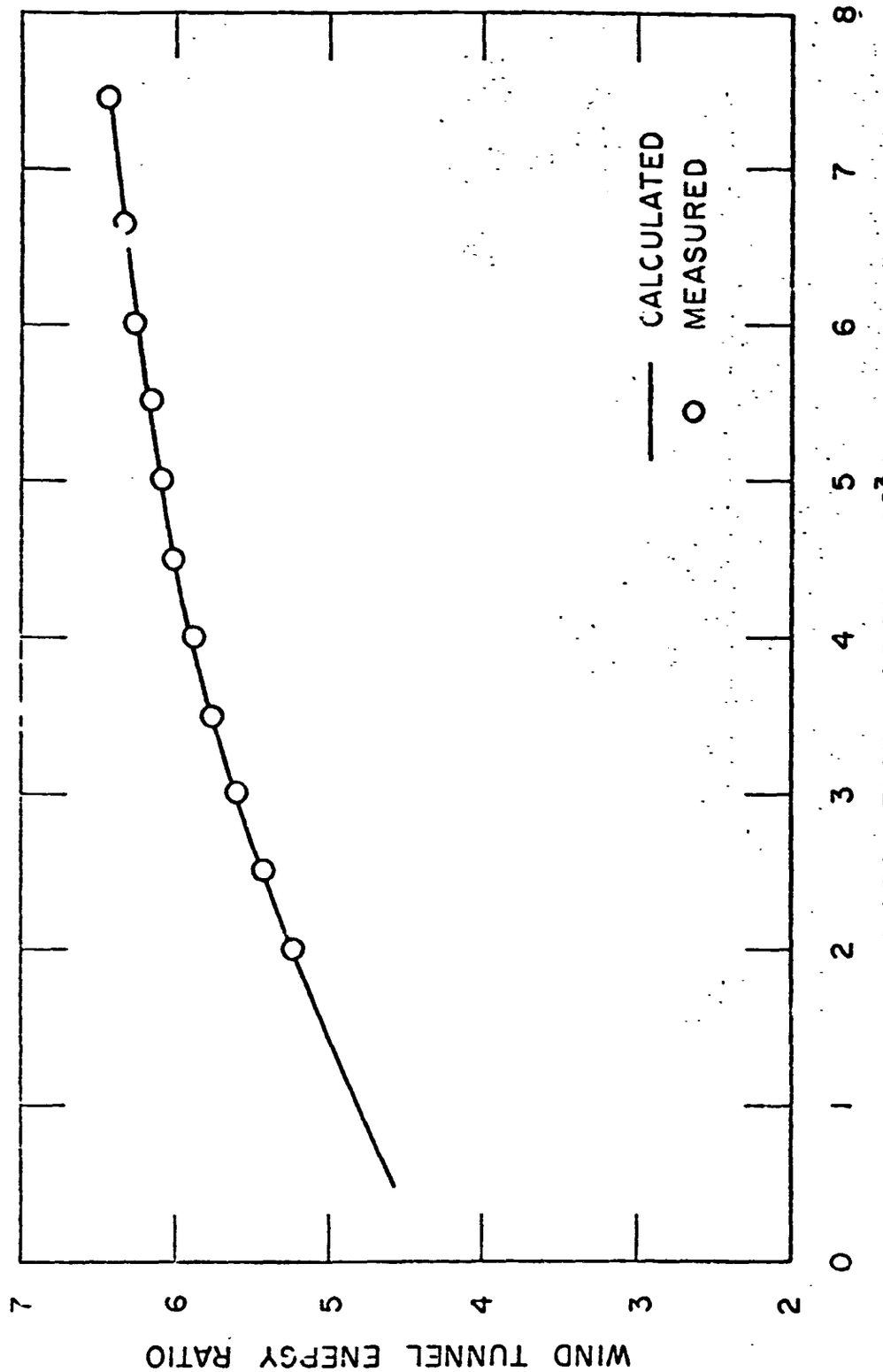

Figure 28. Measured energy ratio versus mass flow

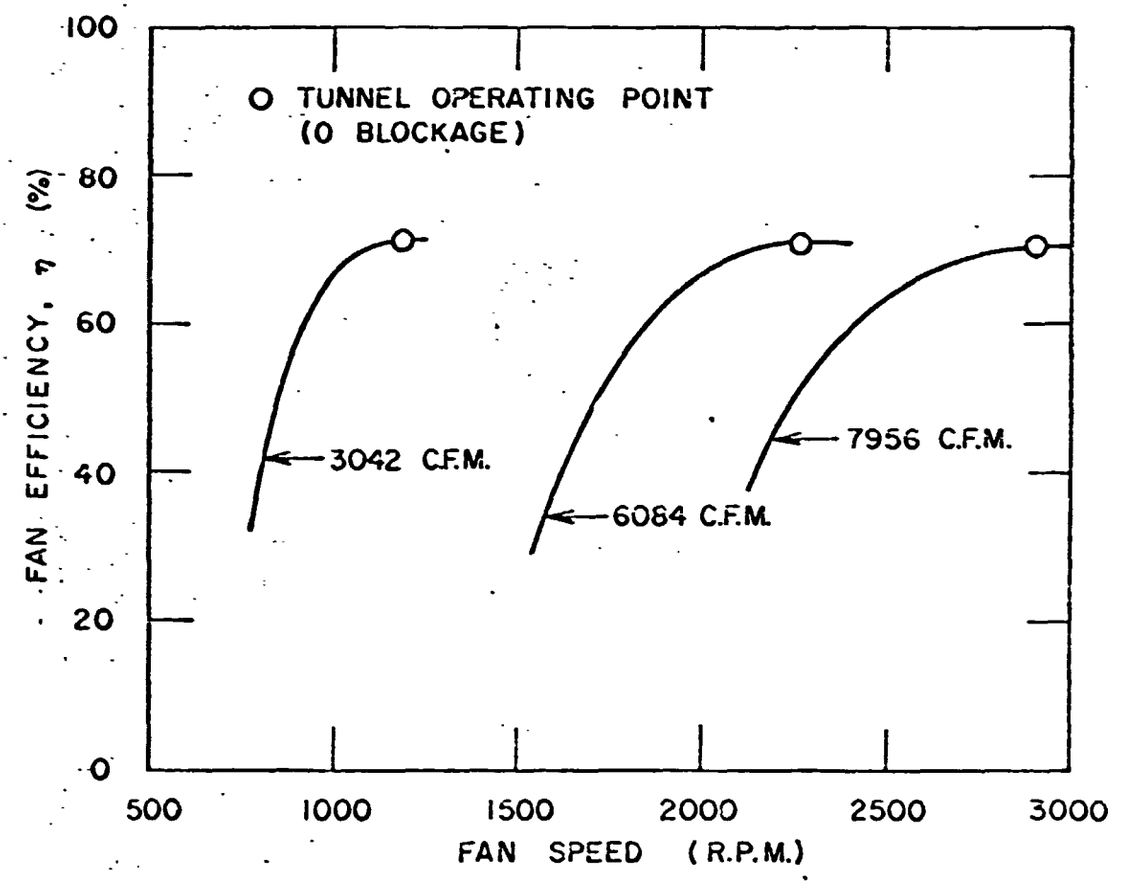

Figure 29. Fan efficiency versus motor speed

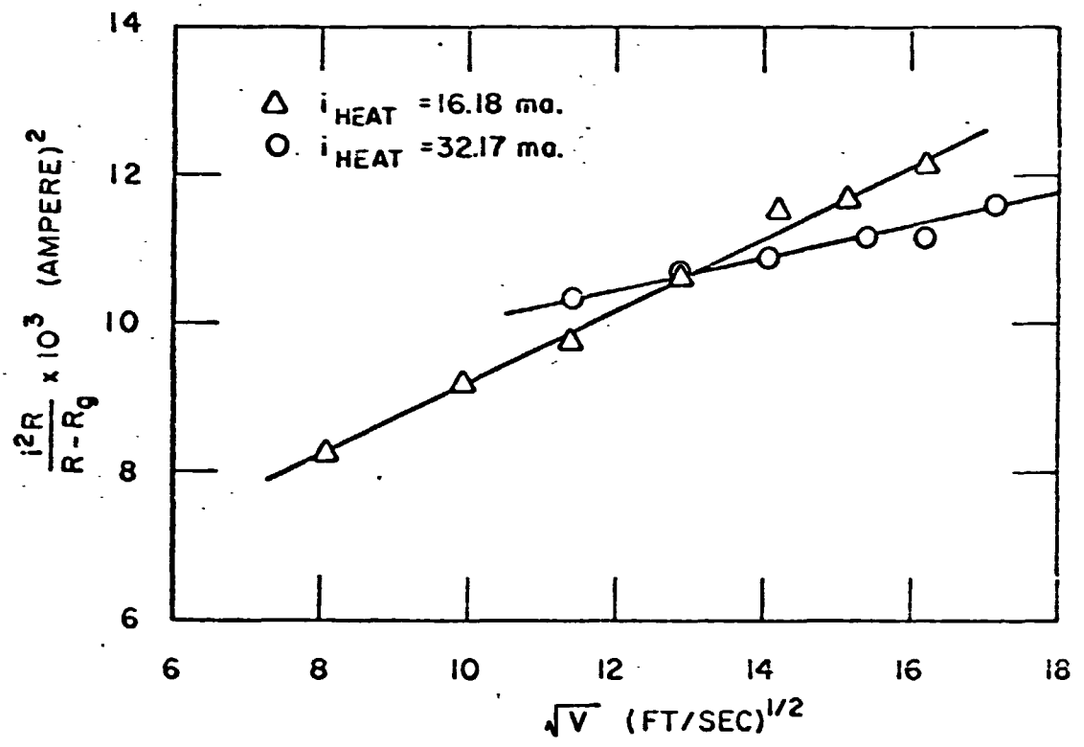

Figure A-1. Hot wire calibration versus freestream velocity

BIBLIOGRAPHY

1. Stephens, T., "Design, Construction and Evaluation of a Magnetic Suspension System for Wind Tunnels," M.I.T. Aerophysics Laboratory TR 136 November 1969.

2. Pope, A., Wind Tunnel Testing, John Wiley and Sons, Inc., November 1958.

3. Pankhurst, R. C. and Hobler, D.W., Wind Tunnel Technique, Pitman Publishing Corp., New York,1952.

4. Schlichting, H., Boundary Layer Theory, McGraw-Hill Book Co., 1955.

5. Roberts, H. E., "Considerations in the Design of a Low Cost Wind Tunnel," Paper presented at the 14th Annual Meeting of the I.A.S., January 1946.

6. Collar, A. R., "The Effect of Gauze on the Velocity Distribution in a Uniform Duct," R and M No. 1867, 1939.

7. Batchelor, G. K., "On the Concept and Properties of Idealized Hydrodynamic Resistance," A.C.A. 13, 1945.

8. Dryden, H. L. and Schubauer, G. H., "The Use of Damping Screens for the Reduction of Turbulence," J.A.S. Vol. 14, p. 221, 1947.

9. Tsien, H. S., "On the Design of the Contraction Cone for a Wind Tunnel," J.A.S., Vol. 10, p. 68, 1943.

10. Ames Research Staff, "Equations, Tables and Charts for Compressible Flow," NACA Report 1135, 1953.

11. Rosenhead, L., Editor, Laminar Boundary Layers, Oxford University Press, 1963.

BIBLIOGRAPHY (Continued)

12. Vlajinac, M. and Gilliam, G. D., "Aerodynamic Testing on Conical Configurations Using a Magnetic Suspension System," M.I.T. Aerophysics Laboratory TR 162 November 1969.

13. Judd, M., Vlajinac, M., Covert, E.E., "Sting-Free Drag Measurements on Ellipsoidal Cylinders at Low Reynolds Numbers" (to be published)

14. Kovasznay, L.S.G., Section F, Physical Measurements in Gas Dynamics and Combustion, Volume IX, High Speed Aerodynamics and Jet Propulsion, Princeton University Press, 1958.